Jovian sodium nebula and Io plasma torus S^+ and brightnesses 2017 – 2023: insights into volcanic vs. sublimation supply

Jeffrey P. Morgenthaler[1], Carl A. Schmidt[2], Marissa F. Vogt[1,2], Nicholas M. Schneider[3], Max Marconi[1]

[1]Planetary Science Institute 1700 East Fort Lowell, Suite 106 Tucson, AZ 85719-2395, USA
[2]Center for Space Physics Boston University Boston, MA 02155, USA
[3]University Of Colorado, Boulder Boulder, CO 80309, USA

Key Points:

- A large set of Jovian sodium nebula and Io plasma torus S^+ images provides context for Io and Jovian magnetospheric studies
- Enhancements in Na and S^+ emission last 1 – 3 months, ruling out insolation-driven sublimation as their driver
- Volcanic plumes likely play a key role in atmospheric escape

Corresponding author: Jeffrey P. Morgenthaler, jpmorgen@psi.edu

Abstract

We present first results derived from the largest collection of contemporaneously recorded Jovian sodium nebula and Io plasma torus (IPT) in [S II] 6731 Å images assembled to date. The data were recorded by the Planetary Science Institute's Io Input/Output observatory (IoIO) and provide important context to Io geologic and atmospheric studies as well as the *Juno* mission and supporting observations. Enhancements in the observed emission are common, typically lasting 1 – 3 months, such that the average flux of material from Io is determined by the enhancements, not any quiescent state. The enhancements are not seen at periodicities associated with modulation in solar insolation of Io's surface, thus physical process(es) other than insolation-driven sublimation must ultimately drive the bulk of Io's atmospheric escape. We suggest that geologic activity, likely involving volcanic plumes, drives escape.

Plain Language Summary

The Planetary Science Institute's Io Input/Output observatory (IoIO) is composed almost entirely of off-the-shelf parts popular with amateur astronomers. IoIO uses special filters to isolate emission from two gasses found around Jupiter: neutral sodium and ionized sulfur. The sodium is thrown out from Io in a vast cloud called the Jovian sodium nebula. The ionized sulfur collects into the Io plasma torus (IPT), a ring-shaped structure centered around Jupiter that wobbles around Io's orbital path. These gasses ultimately come from Jupiter's highly volcanic moon, Io. We see the Na nebula and IPT brighten frequently. This demonstrates that the majority of the material leaving Io comes from whatever drives the frequent brightening events, with volcanic plumes likely playing a key role. Our results challenge a widely held belief in the scientific community, that the majority of the material in the Na nebula and IPT comes from Io's tenuous global atmosphere, which is fed by the sublimation of surface frosts and is relatively stable in time. Our dataset also provides important context for NASA's *Juno* mission and supporting observations that focus on Io volcanism, the material's likely source, and Io's magnetosphere, the material's ultimate destination.

1 Introduction

One of the first hints that Io was somehow releasing material into the Jovian magnetospheric environment in large amounts compared to the other Galilean satellites came from spectroscopic observations of sodium D1 (5896 Å) and D2 (5890 Å) emissions that were time variable, broad, and in a ratio suggesting optically thick gas (R. A. Brown & Chaffee, 1974). Kupo et al. (1976) conducted spectroscopic studies of S^+ in the [S II] 6717 Å and 6731 Å doublet in the orbital plane of Io and detected extended emission corotational with Jupiter. As *Voyager I* approached Jupiter, Extreme ultraviolet (EUV) emission from S III, S IV, and O III resolved into a torus-like structure encircling Jupiter, dubbed the Io plasma torus (IPT; Broadfoot et al., 1979). The potential source of the material escaping Io was first hinted at when Io itself was also seen to be intermittently bright at a particular orbital phase angle in the 3 – 5 μm region of the infrared spectrum, with volcanic activity being one of several possible explanations offered (Witteborn et al., 1979). Volcanic activity on Io was subsequently unambiguously confirmed by *Voyager* 1 images of plumes and volcanic surface features (Morabito et al., 1979; Smith et al., 1979). This volcanism gives rise, either directly or indirectly, to an SO_2 dominated atmosphere (Pearl et al., 1979; Kumar, 1979; de Pater et al., 2021) with minor constituents, including NaCl (Lellouch et al., 2003; McGrath et al., 2004; Moullet et al., 2010; Redwing et al., 2022).

Io's atmosphere undergoes several reactions with material in the IPT, resulting in detectable effects. For majority species S and O, change exchange, sputtering, and electron impact ionization are important processes for removing atmospheric material (e.g.,

McGrath & Johnson, 1987; Smyth & Combi, 1988b, 1988a; Thomas et al., 2004; Schneider & Bagenal, 2007; Dols et al., 2008, 2012; Smith et al., 2022), resulting in a roughly torus-shaped neutral cloud confined to Io's orbital plane and mapped in the EUV at O I 1304 Å (Koga et al., 2018a). IPT electron impact ionization of this neutral cloud is the primary process by which the IPT receives new material, with direct ionization in Io's atmosphere providing only a minor component (Dols et al., 2008, 2012). The canonical value of $\sim$1 ton s^{-1} of material flowing into the IPT from Io has been estimated using the IPT's total EUV power output and a simple geometric model of the EUV emission region (e.g., Broadfoot et al., 1979; Schneider & Bagenal, 2007).

The path that sodium-bearing material takes as it escapes Io's atmosphere is different, thanks to the low ionization potential of any sodium-containing molecule, NaX. For these molecules, impact ionization and charge exchange processes are very efficient (e.g., Schneider & Bagenal, 2007). Pickup NaX ions generated in Io's exosphere that promptly neutralize and dissociate create a directional feature, the "jet," that points radially outward from Io and flaps up and down in synchrony with the IPT (Pilcher et al., 1984; Wilson & Schneider, 1999; Burger et al., 1999, see also animations accompanying Figure 1). A more extended structure, dubbed the "stream," has a similar radial morphology and behavior relative to IPT modulation, but extends for several hours in Jovian local time downstream of Io's position. This comes from NaX^+ ionized in Io's exosphere by IPT plasma and swept downstream in the plasma flow before they neutralize (Schneider et al., 1991; Wilson & Schneider, 1994). IPT NaX^+ ions that dissociate produce neutral fragments that are ejected from the IPT at an average of $\sim$70 km s^{-1}, which is the Jovian corotational velocity at the IPT. This velocity is above Jupiter's escape velocity. Thus, neutral Na is detected at distances >500 Jovian radii (R_j) from Jupiter (Mendillo et al., 1990). All these neutral sodium emission features are known collectively as the Jovian sodium nebula and are well-described by Monte Carlo modeling techniques (Wilson et al., 2002). The Jovian sodium nebula has been the subject of several long-term studies using ground-based coronagraphic techniques (Mendillo et al., 2004; Yoneda et al., 2009, 2015; Roth et al., 2020; Morgenthaler et al., 2019, and this work).

Except for the study presented here, long-term observations of the IPT from ground-based observatories have been limited. The longest continuous study to date covered a full Jovian opposition using a spectroscopic technique (M. E. Brown & Bouchez, 1997). Ground-based IPT imaging campaigns using coronagraphic techniques have typically lasted a few weeks per opposition, though some have extended over several oppositions (Schneider & Trauger, 1995; Woodward et al., 2000; Nozawa et al., 2004; Kagitani et al., 2020). These ground-based observations concentrate on the bright [S II] emissions of the 6717 Å, 6731 Å doublet, which are excited by IPT thermal electrons. A significant amount of structure is seen in high-resolution IPT images: a dense "ribbon" near Io's orbit is separated by a gap from the more disk-like "cold torus," closer to Jupiter (e.g. Schneider & Trauger, 1995). There is evidence that diffusion proceeds inward from the ribbon to the cold torus (Herbert et al., 2008). Long-term spectro-imaging observations of EUV emission of the IPT have been conducted from *Voyager*, *Cassini*, and *Hisaki* (Broadfoot et al., 1979; Steffl et al., 2004; Yoshioka et al., 2014). This emission, known as the "warm torus," is more extended radially and vertically than the ribbon. The EUV emissions are excited by suprathermal electrons and have been used to study radial transport in the IPT, providing evidence that the total residence time of material in the IPT is 20 – 80 days (Bagenal & Delamere, 2011; Hess et al., 2011; Copper et al., 2016; Tsuchiya et al., 2018). Once material has left the IPT, it rapidly spirals outward in a few days (Bagenal & Delamere, 2011). Thus, long-term monitoring of the IPT, such as that presented here, provides critical context to any study of Jupiter's broader magnetosphere, such as that conducted by NASA's *Juno* mission (Bolton et al., 2017) and supporting observations (Orton et al., 2020, 2022).

In this work, we present the first results of a combined Jovian sodium nebula and IPT monitoring campaign, conducted since March 2017 by the Planetary Science Institute's Io Input/Output observatory (IoIO). The coronagraphic observations are described in §2 and §3 provides the methodology used to reduce the data. Section 4 presents the primary results of our study, which is a time history of the surface brightnesses of the Na nebula and IPT (Figure 4). This time history shows 1 – 2 brightness enhancements per 7-month observing season, each lasting 1 – 3 months, such that emissions are seldom found in a quiescent state. In §5 we compare our results to previous studies, noting that although none of the previous workers reported such frequent activity in the Na nebula and IPT, all are consistent with it. In §6, we use the IoIO data to rule out solar insolation-driven sublimation of Io's surface frosts as the primary driver of material from Io's atmosphere, showing instead that geologic processes must be involved. We then review the existing evidence that connects enhancements in material escape from Io's atmosphere with volcanic plume activity and discuss implications for the transport of material. A summary and concluding remarks are provided in §7. In §8, we suggest additional uses for the IoIO dataset, including providing support for current and planned missions to Jupiter.

2 Observations

All observations presented here were conducted with the Planetary Science Institute's Io Input/Output observatory (IoIO). IoIO consists of a 35 cm Celestron telescope feeding a custom-built coronagraph, described by Morgenthaler et al. (2019). Since the publication of that work, both the observatory hardware and control software have been upgraded, enabling fully robotic acquisition of Jovian sodium nebula and IPT [S II] on- and off-band images, regular photometric observations of Burnashev (1985) spectrophotometric standard stars in all filters, and observations of telluric sodium foreground emission. Bias, dark and sky flat images are also periodically recorded. Since 2017-03-09, IoIO has contemporaneous recorded Na 5890 Å nebula and IPT [S II] 6731 Å observations on over 550 nights, with over 2300 Na images and over 8300 [S II] images collected. The observatory has been operated on another ∼500 nights in support of other Planetary Science Institute projects (e.g., Adams et al., 2023) and pilot studies, increasing the number of spectrophotometric calibrations and time coverage of telluric Na emission, which provides a time-variable foreground emission (e.g., Plane et al., 2018).

3 Data Reduction

3.1 General Considerations

All IoIO data are reduced pipeline-style using the software enumerated in the Open Research section. The Burnashev (1985) spectrophotometric observations show each filter in our filter library provides stable zero points and extinction coefficients over the length of our study, modulo random nightly variations due to variation in atmospheric transparency, which we ignore in our current analyses, using instead the biweight location (Tukey, 1977), of all the measurements of each filter. The biweight location, ζ_{biloc}, is defined as:

$$\zeta_{biloc} = M + \frac{\sum_{|u_i|<1} (x_i - M)(1 - u_i^2)^2}{\sum_{|u_i|<1} (1 - u_i^2)^2} \tag{1}$$

where x is the data, M is the median of the data. The quantity u_i is:

$$u_i = \frac{(x_i - M)}{c * MAD} \tag{2}$$

where c is a tuning constant, set to 9 in our case, and MAD is the median absolute deviation:

$$MAD = \text{median}(|(x_i - \overline{x}|) \tag{3}$$

The biweight location is a more robust statistical measure of the central location of a distribution than the median, particularly for data not distributed as a Gaussian (Beers et al., 1990). Surface brightnesses are expressed in rayleighs (R), where:

$$1\ R = \frac{10^6}{4\pi}\ \text{photons cm}^{-2}\ \text{sec}^{-1}\ \text{sr}^{-1} \tag{4}$$

Astrometric solutions of our images, together with high-quality JPL HORIZONS ephemerides (Giorgini et al., 1996) enable high-precision alignment of on- and off-band images before subtraction of the off-band images. Subtraction of the off-band images effectively removes Jupiter's scattered continuum light from the on-band images. When astrometric solutions using field stars fail, the position of Jupiter on the coronagraph neutral density (ND) filter is used to establish the astrometric center of the image, with the clock angle determined by the previous successfully solved image. As expected from our stellar calibrations, we found the ratio between our on- and off-band sky flats gave stable results over the lifetime of the project. Thus, we used the biweight location of all ratios to scale the off-band images before subtraction from the on-band. Sample reduced images are shown in Figure 1.

We note that our calibration procedure is a significant improvement over the technique used by Morgenthaler et al. (2019), which relied on the image of Jupiter through the ND filter for surface brightness calibration. As discovered after the installation of a larger and filter wheel in 2019, Jupiter's detected brightness is subject to an unexpected Fabry Pérot effect between the narrow-band and ND filters, with each narrow-band filter providing a different magnitude of effect. Our current procedure avoids this issue by using the stellar and flat-field calibrations described above.

In order to establish a time-sequence of the Na nebula and IPT brightnesses, we first rotate the images reduced by the procedure above into the plane of the IPT centrifugal equator using the relation:

$$\alpha = -A \times\ cos(\lambda_{\text{III}} - P) \tag{5}$$

where α is the angle between the Jovian rotational axis and the perpendicular to the IPT centrifugal equator, λ_{III} is the sub-observer System III longitude, A is the amplitude of the oscillation of the centrifugal equator and P is the λ_{III} longitude of the intersection of the magnetic and equatorial planes. For this work, we used $A = 6.8°$ (Moirano et al., 2021) and $P = 290.8°$ (Connerney et al., 1998). Values of $A = 6.3°$ (Phipps & Bagenal, 2021) and $P = 286.61°$ (Connerney et al., 2018) could also be used, and would result in trivial differences in our extracted surface brightnesses.

3.2 Na Nebula

As shown by previous work (§1) and the Na nebula animations accompanying Figure 1 in the online journal, the bulk of the bright jet and stream emission follow Io in its 42 hour orbit and flap up and down with each 9.925 hr Jovian rotation. To minimize the effects of this high variability when extracting surface brightnesses from individual Na nebula images, we rotate each image by α, as described above, and divide the resulting image into horizontal apertures distributed vertically from the IPT centrifugal plane,

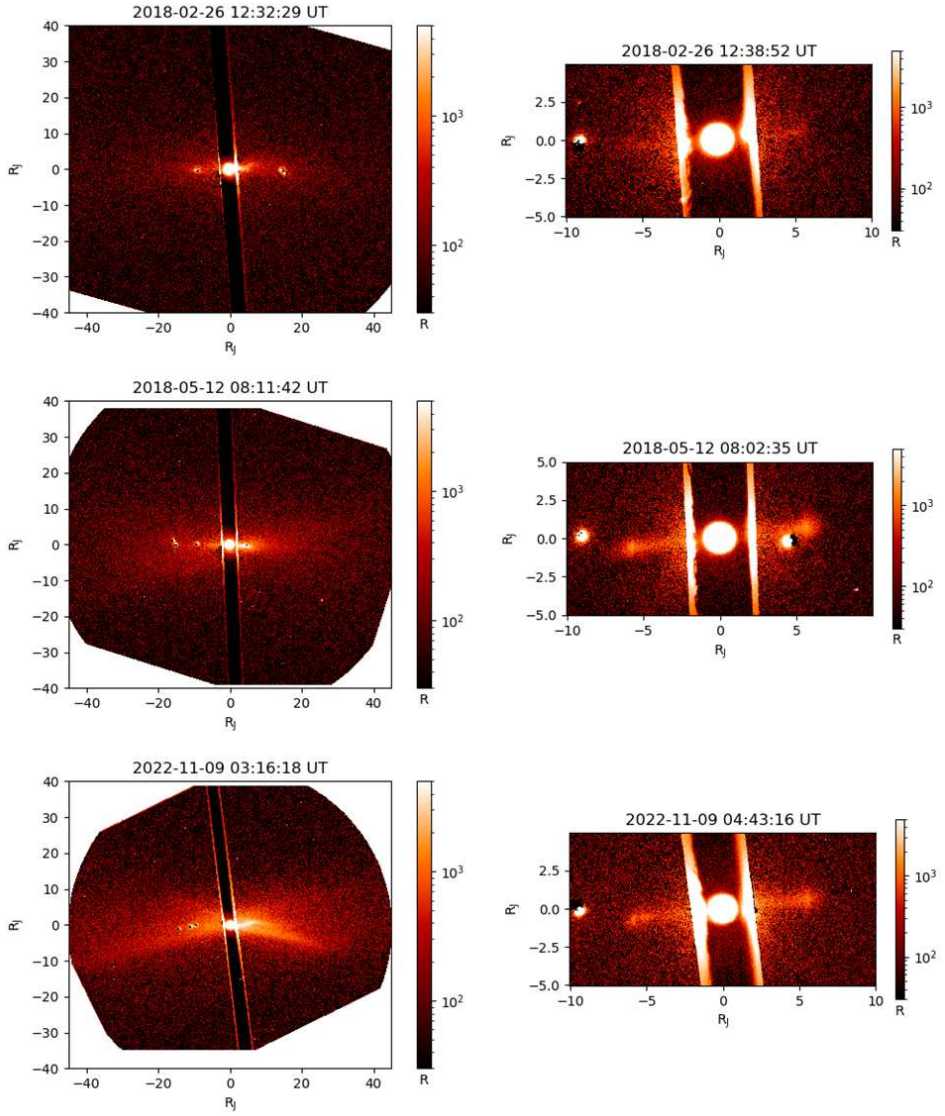

Figure 1. Sample IoIO Na nebula (left column) and IPT [S II] 6731 Å (right column) images. The top row shows images recorded just before the large 2018 enhancements in Na nebula and IPT emission (see Figure 4), the middle row images recorded near the 2018 Na nebula and IPT peaks in emission and the bottom row images recorded near the 2022 peaks. Animations are provided in the on-line journal.

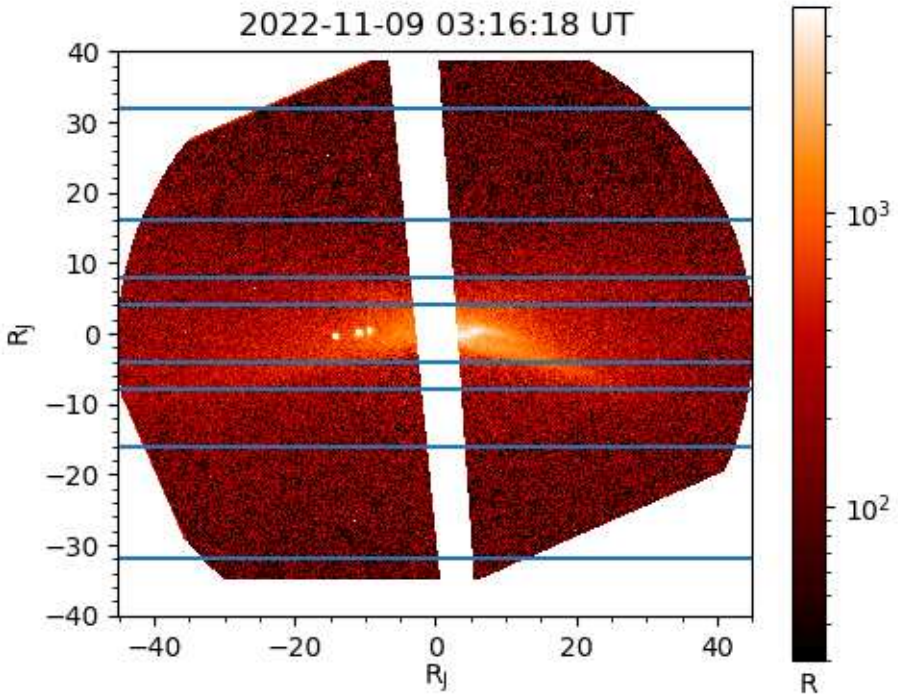

Figure 2. Sample Na nebula image illustrating reduction steps described in §3.2. The blue lines indicate boundaries between apertures used to extract surface brightness values as a function of vertical distance from the IPT centrifugal plane. The boundaries between apertures are defined by the following vertical distances from the IPT centrifugal plane: 4 R_j – 8 R_j, 8 R_j – 16 R_j, and 16 R_j – 32 R_j, with the average distances from the plane of each pair of apertures used for subsequent identification (e.g., see legend of Figure 4, top). Masked areas are shown in white.

as shown in Figure 2. The ND filter and area beyond the edge of the narrow-band filters are masked, as are pixels with values above the non-linear point of the CCD, with a larger mask area applied around Galilean satellites. The average surface brightness in each aperture is calculated by totaling the individual surface brightnesses of the unmasked pixels and dividing by the total number of unmasked pixels. The final surface brightness for a given distance from the IPT centrifugal plane is the average of the surface brightnesses of the pair of apertures located at that distance above and below the plane.

3.2.1 Removal of Telluric Sodium Contamination

Telluric sodium emission provides a time-varying and, at times, substantial field-filling component to our Na nebula images. We attempted to remove this emission using an empirical model constructed from our multi-year dataset of telluric sodium emission observations. The model accounted for airmass effects, solar scattering angle, and seasonal effects. However, after subtraction of the model, the time sequence of Na nebula surface brightnesses was still quite noisy. Thus, we instead subtract the average surface brightness of emission >32 R_j above and below the centrifugal plane from the extracted surface brightnesses of each image. As a result, the variation induced by telluric emission was greatly diminished. A final step in the Na nebula reduction is to compute

the biweight location of all of the measurements at each distance on each night. The results are plotted together with 21-point moving median filter in Figure 4 (top).

A byproduct of our telluric sodium removal technique is to induce an intensity-dependent error of the order $\sim 5\,\mathrm{R}$ – $\sim 25\,\mathrm{R}$ in our quoted Na nebula surface brightnesses. This is because our telluric removal procedure effectively assumes that the brightness of the Na nebula is zero at the edge of the IoIO FOV. However, as shown by larger-field images (Mendillo et al., 2004; Yoneda et al., 2009, 2015), the emission >30 $\mathrm{R_j}$ above and below Jupiter's equatorial plane varies from $< 5\,\mathrm{R}$ to $\sim 25\,\mathrm{R}$, depending on whether or not the nebula is enhanced. This effect could be corrected using a model of the Na nebula emission, however, doing so would not affect the results of our current study.

3.3 IPT

As shown by comparing Figure 1 (lower right) to the IPT image in Figure 3, rotating by Equation 5 provides a natural coordinate system for extracting brightness values of the ansas (edges, Latin: "handles") of the IPT. As described in §1, the [S II] 6731 Å ansas primarily capture the IPT ribbon emission. We extract the average surface brightness from each ribbon feature using the two-step process shown graphically in Figure 3. Specifically, starting from the rotated image, we define ansa extraction regions that extend radially 4.75 $\mathrm{R_j}$ to 6.75 $\mathrm{R_j}$ from Jupiter and ±1.25 $\mathrm{R_j}$ above and below the IPT centrifugal equator (white boxes). Radial profiles of the emission in the white boxes are shown in the bottom row. These profiles are generally well-fit by a Gaussian plus sloping continuum of the form:

$$f(x) = Ae^{\frac{-(x-x_0)^2}{2\sigma^2}} + P_0 + P_1 x \tag{6}$$

where A is the peak surface brightness of the Gaussian component of the radial profile, x_0 is the ribbon radial distance from Jupiter, σ is the width of the ribbon, and P_0 and P_1 are the coefficients of the linear background. The ±1-σ limits of these Gaussians are used to define the radial limits of the region used to extract vertical profiles, shown in the top row, outside plots. Equation 6, with $P_1 = 0$, is used to fit the vertical profiles. The Gaussian component of this function is integrated to arrive at an average ribbon intensity of $A\sigma\sqrt{2\pi}$. This is converted to an average surface brightness by dividing by σ. Occasionally, the data are of high enough quality and the torus configured such that cold torus is resolved. This is the case for the dawn (left) ansa and results in a small peak inside of the ribbon. We ignore the effect of this feature on our fits, since the simple sloping continuum plus Gaussian provides an adequate a foundation for determining the region over which to extract vertical profiles. As shown in the Figure, the vertical profiles are well-described by Equation 6, with $P_1 = 0$. The total area of the Gaussian components of each fit is then used to establish the average surface brightness of each ribbon. If an extraction area contains saturated pixels from any nearby Galilean satellite, it is excluded from the analysis. Fits that result in ribbon peak positions outside of the range 5.0 $\mathrm{R_j}$ – 6.5 $\mathrm{R_j}$ or peak widths outside the range 0.1 $\mathrm{R_j}$ – 0.5 $\mathrm{R_j}$ are discarded. In this way, our extractions are able to adjust for varying observing conditions and the intrinsic variability in the IPT ansa morphology (e.g., Schneider & Trauger, 1995) and reliably discard pathological cases. The time history of the average ribbon surface brightnesses, together with a 21-point running median filter of the dusk ribbon points are plotted in Figure 4 (bottom). On timescales of weeks to months, all other parameters of the fits roughly scale with ribbon surface brightness, except for the radial peak positions of the ribbon. This behavior is expected because all of the parameters of the fits, except the radial peak positions, are sensitive to the total amount of material in the IPT, whereas the radial positions of the ribbon are determined by physical effects outside of the IPT (e.g., Barbosa & Kivelson, 1983; Ip & Goertz, 1983, see also §8).

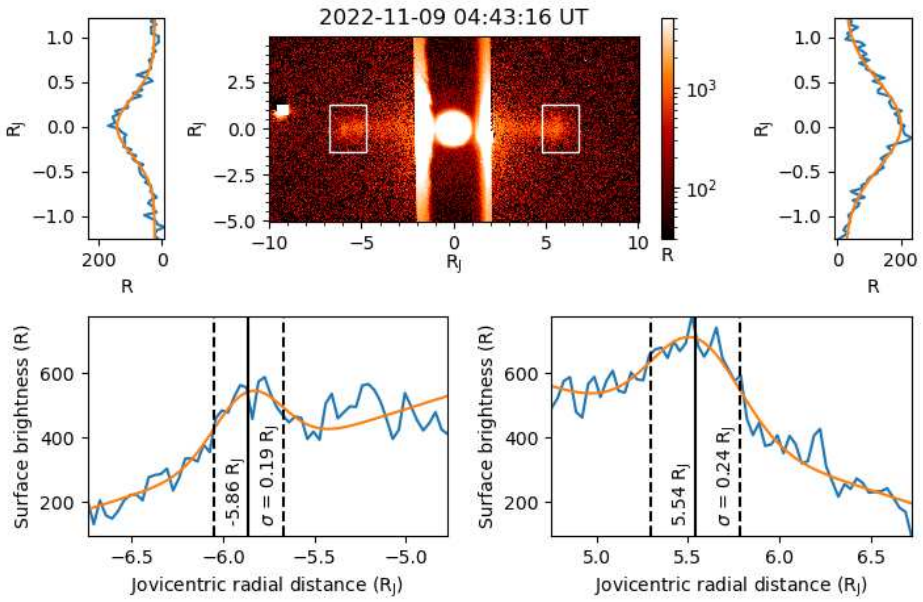

Figure 3. Graphical depiction of [S II] ribbon surface brightness extraction process described in §3.3. An IPT image rotated into the reference frame of the IPT centrifugal equator is shown in the top, middle panel. Radial profiles of the ansas are shown in the bottom row, fit by Equation 6. The 1-σ limits indicated on these plots define the edges of regions between which the vertical profiles are computed (top row, outer plots). The average surface brightness of each ribbon is the integral of the Gaussian component of the fit of the corresponding vertical profile.

We note that, as derived, the absolute values of the dawn ribbon surface brightness values shown in Figure 4 (bottom) are artificially low because, at the blueshift of the dawn ribbon, IPT emission falls outside of the central bandpass of the [S II] 6731 Å filter as measured in a collimated beam. This effect can be corrected using a velocity-dependent IPT map, the [S II] filter transmission curve, and consideration of the effects of the telescope's F/11 light paths on the filter's total transmission. However, making these corrections would not affect the results of our current study.

4 Results

We anticipate the IoIO data will be very useful for correlative studies for observations focusing on Io and the effect that material escaping Io has on Jupiter's magnetosphere, such as afforded by NASA's *Juno* mission (Bolton et al., 2017) and supporting observations (Orton et al., 2020, 2022). To that effect, the surface brightness points shown in Figure 4 have been archived at Zenodo (Morgenthaler et al., 2023). In this paper, we focus on what the data themselves can say about the physical processes that drive material escape from Io's atmosphere.

Our 6-year time sequence of Jovian Na nebula and IPT [S II] 6731 Å ribbon brightnesses (Figure 4) shows considerable modulation in each emission line as a function of time. During each ∼7-month observing window, at least 1 – 2 enhancements, each lasting 1 – 3 months are seen. Very little time is spent in a quiescent state. Visual inspection of Figure 4 reveals that the average values of the Na nebula and IPT surface brightnesses are determined by the enhancements, rather than any quiescent value. To quantify this finding we compute the Tukey (1977) biweight distribution (Equation 1) of the

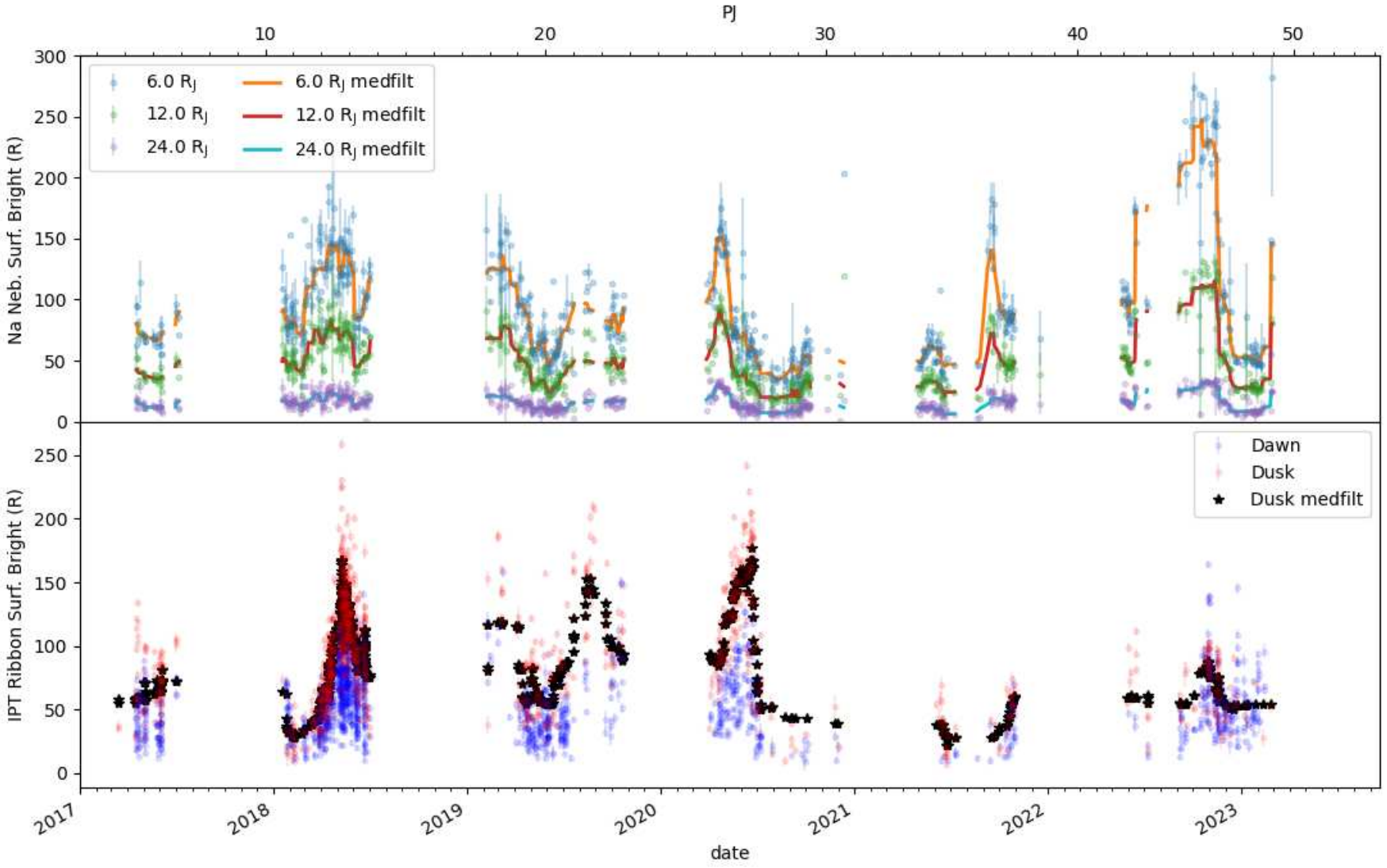

Figure 4. Top: Time sequence of surface brightnesses in Jovian sodium nebula at three distances from the plasma torus equatorial plane. Bottom: Time sequence of IPT ribbon average surface brightnesses. A running median filter, 21 points wide, is applied to each Na aperture and the dusk ribbon brightnesses.

measurements presented in Figure 4. Recall from §3.1 that the biweight distribution is a more robust statistical measure of the central location of a distribution than the median or average. The biweight distribution values of the Na nebula points are 80 R, 50 R and 15 R in the 6 R_j, 12 R_j, and 24 R_j apertures, respectively. Compare this to low values of approximately 30 R, 20 R, and 5 R. Similarly, the biweight distributions of the ribbon brightnesses are 50 R and 90 R for dawn and dusk, respectively, with minima of 15 R and 30 R.

Visual inspection of Figure 4 also shows a quasi-contemporaneous relationship between the Na nebula and IPT enhancements. For instance, the relative timing between the peaks of the 2018 Na nebula and IPT enhancements is significantly different than that seen in 2020. And the fall 2022 Na nebula enhancement is particularly bright compared to other Na nebula enhancements, yet the IPT enhancement during that time period is particularly weak compared to other years. This type of behavior has not been reported before.

We discuss the implications of our results in §6. But first, we compare our results to those of previous studies, which provide valuable context to our discussions.

5 Comparison to previous studies

IoIO occupies a unique niche in sensitivity, which ideally suits it to study of the modulation of material flow from Io into the broader Jovian magnetosphere. The 35 cm telescope aperture of IoIO was chosen to be comparable to the smallest apertures that have successfully imaged the IPT (Nozawa et al., 2004). This has allowed us to reliably capture, at modest cost, a 6-year history of the modulation in the IPT [S II] 6731 Å ribbon brightnesses (presented here) and positions (to be presented in a subsequent work). Our equipment choice limited the FOV of the instrument to 0.4°, which is much smaller than the 2.5° – 7° FOV of long-term previous coronagraphic Na nebula studies (Mendillo et al., 2004; Yoneda et al., 2009, 2015; Roth et al., 2020). However, the narrower FOV of IoIO affords it much greater sensitivity to emission close to Io, as evident by comparing the left columns of our Figure 1 to Figure 1 of Mendillo et al. (2004) and Figures 2 of Yoneda et al. (2009, 2015). This feature of the IoIO Na nebula observations will allow us to conduct detailed morphological studies of the jet and stream in future work.

5.1 Sodium-related studies

The outer portions of the IoIO FOV overlap with the inner portions of the images recorded by other wide-field Na nebula studies (Mendillo et al., 2004; Yoneda et al., 2009, 2015; Roth et al., 2020), allowing direct comparison. For instance, the peak intensity of the fall 2022 Na nebula enhancement detected by IoIO roughly compares to the peak intensities in the 2007 and 2015 enhancements captured by Yoneda et al. (2009, 2015). The Roth et al. (2020) study is useful, since it provides a time-history of Na nebula brightnesses measured with the same coronagraph used in the Yoneda et al. (2015) work for a 4-month interval in 2017 during which no enhancement was reported. Nevertheless, modulation at the ∼10 R level in daily values (∼5 R in the half-month averages) is seen. This is comparable to the variation seen in the IoIO dataset during the 2018 enhancement. The greater sensitivity of the IoIO coronagraph to emission closer to Jupiter makes variation of this magnitude much easier to detect. This implies that periods formerly identified as quiescent in the Yoneda et al. (2015) dataset may, in fact, contain enhancements. By that interpretation, the period highlighted in the Roth et al. (2020) appears to be capturing the low point between two enhancements.

Spectroscopic observations conducted at the Lick observatory over the entire 1995 Jovian opposition (M. E. Brown, 1994; M. E. Brown & Bouchez, 1997) are also useful for comparison. This work captured an enhancement in both the Na 5890 Å doublet and

[S II] 6731 Å (see also Sections 5.2 – 5.3). The 10″ spectrograph slit was aligned along the centrifugal equator, with peak emission averaged along the slit reaching levels of 400 R – 800 R. In order to compare to our data, we extend the aperture extraction procedure outlined in §3.2 using apertures progressively closer to the centrifugal plane following the same geometric sequence. We stopped decreasing the aperture size when the emission brightness increased by <10%. The resulting aperture extended 0.5 R_j above and below the centrifugal plane and resulted in peak brightnesses of 200 R – 300 R during the years 2017 – 2021 and 630 R in 2022. This suggests that the 1995 Na enhancement captured by M. E. Brown and Bouchez (1997) was comparable in size to the 2022 enhancement shown in Figure 4 (upper panel).

Also important to mention are the *Galileo* dust detector measurements acquired 1996 – 2003 (Krüger, Geissler, et al., 2003). There is evidence that the dust comes from Io (Graps et al., 2000; Krüger, Horányi, & Grün, 2003), is composed almost entirely of NaCl (Postberg et al., 2006) and has its origin from Io volcanic plumes (Krüger, Geissler, et al., 2003). Further evidence shows that $NaCl^+$ is an important pathway for Na escape from Io's atmosphere (Grava et al., 2014; Schmidt et al., 2023). This suggests that variation seen in our Na nebula dataset and others should be echoed in the *Galileo* dust detector data. Krüger, Geissler, et al. (2003) used a simple geometric model of dust emission from Io to translate dust detector count rates into the flux of dust from Io (their Figure 2). As discussed by Krüger, Geissler, et al. (2003), the *Galileo* orbit precluded continuous measurements of the dust streams before mid 2000. However, beginning after this time, there was a large, well-covered enhancement that lasted ∼6 months. Subsequent enhancements in the calculated Io dust flux last ∼1 – ∼3 months and have smaller amplitudes than the 2000 enhancement. The magnitudes of the enhancements are 1 – 4 orders of magnitude, which is much larger than those seen in sodium nebula data. Full treatment of the reasons for the difference in magnitude seen between the different measurement methods is beyond the scope of this work. Rather, we point out that the durations of the enhancements in the derived dust flux from Io is comparable to those observed in the Jovian sodium nebula (M. E. Brown & Bouchez, 1997; Yoneda et al., 2009, 2015, and this work).

5.2 IPT studies

Previous studies of IPT [S II] 6731 Å emission show peak ribbon brightness values in the ∼100 R – ∼1000 R range in individual measurements (e.g., Morgan, 1985; Oliversen et al., 1991; Jockers et al., 1992; Woodward et al., 1994; Schneider & Trauger, 1995; Thomas et al., 2001; Nozawa et al., 2004; Yoneda et al., 2009; Schmidt et al., 2018). As described in §3.3, the values shown in Figure 4 are the average surface brightness of each ribbon derived using a two-step Gaussian fitting procedure, with one Gaussian used to isolate emission in the radial direction and one to compute the average surface brightness in the vertical. To convert from averages over the Gaussian functions to peak values, we multiply by 2π, one factor of $\sqrt{2\pi}$ for the integral over the vertical Gaussian and another factor of $\sim\sqrt{2\pi}$ to account for the summation between the $\pm1\sigma$ limits of the radial Gaussian. Following our 21-point moving averages, this yields peak values of ∼200 R – ∼900 R, with individual points ranging from ∼50 R to ∼1200 R. We take this to be good agreement with previous studies and therefore independent validation of our stellar calibration procedure.

The only other published study of IPT [S II] 6731 Å emission lasting more than a few weeks during a single Jovian opposition is the companion of the spectroscopic Na nebula observations collected in 1995 at the Lick observatory, discussed in §5.1 (M. E. Brown, 1994; M. E. Brown & Bouchez, 1997). That study captured an IPT enhancement that lasted ∼2.5 months. The emission pre- and post enhancement was ∼200 R and the emission was ∼400 R at its peak. The factor of ∼2 difference between the pre/post and peak values is comparable to the broad enhancement partially captured at the beginning of

the 2019 Jovian opposition. In other words, within the range observed over our 6-year study.

Also useful for comparison are the two long-term studies of the warm torus that have been conducted in the EUV, one by *Cassini* and one by *Hisaki* (e.g., Steffl et al., 2004; Yoshikawa et al., 2017). Comparison of the surface brightnesses seen in the EUV warm torus observations to the surface brightness of the [S II] 6731 Å observations of the ribbon region would require detailed IPT modeling that is beyond the scope of this work. Thus, we limit our discussion to the duration of the enhancements. During the duration of its observations, *Cassini* captured two enhancements in emissions from ionization states of S and O lasting of order 1 – 3 months, one in late 2000, the other in early 2001. During its multi-year observing campaign *Hisaki* saw one large enhancement that lasted ∼3 months in 2015. Smaller amplitude modulations in the *Hisaki* data have also been noted (Roth et al., 2020). These enhancement durations are comparable to those seen in the IoIO data.

5.3 Contemporaneous Na nebula and IPT studies

Two previous studies reported contemporaneous Na nebula and IPT enhancements (M. E. Brown & Bouchez, 1997; Tsuchiya et al., 2018). These studies, and related work, concentrated on the detailed behavior of the observed emission during the enhancements and the implications for physical processes occurring within the IPT and broader Jovian magnetosphere (e.g., Yoshikawa et al., 2017; Kimura et al., 2018; Hikida et al., 2018; Yoshioka et al., 2018; Tsuchiya et al., 2018; Hikida et al., 2020; Roth et al., 2020; Tao, Kimura, Badman, Murakami, et al., 2016; Tao, Kimura, Badman, André, et al., 2016; Tao et al., 2018, 2021). Such in-depth study of individual enhancements is beyond the scope of our current work. Rather, we note for comparison to our data, that for both the 1995 and 2015 enhancements, there was delay of ∼4 weeks between the peak in the Na nebula and IPT S^+ emissions, even though in the 2015 case, the S^+ emissions were from the ribbon region and detected via the [S II] 6731 Å line and in the 2015 case, the emissions were from the warm torus and detected via the S II 765 Å line. Because different regions of the torus were studied in the two cases, comparison of the relative strengths of the IPT enhancements requires modeling that is beyond the scope of this effort. Thus, we are not currently able to use these studies to corroborate our observation that the relative strengths of the Na nebula and S^+ enhancements can vary significantly with time.

6 Discussion

Our study has a unique combination of sensitivity, cadence and duration that has enabled it to determine that the Na nebula and IPT are frequently in states of enhancement and that the enhancements in the two species have a quasi-contemporaneous relationship. When interpreted within the context of previous studies, the former result allows us to rule out solar insolation-driven sublimation as the primary mechanism driving Io atmospheric escape; the later provides insights into the most likely mechanism – volcanism – and the subsequent path sodium- and sulfur-containing materials take through and out of Io's atmosphere. Our discussion begins with atmospheric escape.

6.1 Response of sodium nebula and IPT to Io atmospheric escape

As reviewed in §1, Io's atmosphere is removed by interaction with the IPT via charge exchange, sputtering, and electron impact ionization to fill the neutral clouds on timescales of hours (e.g., Smyth & Combi, 1988a; Dols et al., 2008, 2012; Smith et al., 2022). The apertures used to extract Na nebula surface brightnesses (Figure 2) are primarily filled by sodium traveling near IPT's $\sim 70\,\mathrm{km\,s^{-1}}$ corotation velocity. The residence time of this material in the IoIO FOV is ∼11 hours. Furthermore, we have chosen the apertures

that integrate over the effect of Jupiter's ∼10 hr rotation period and Io's ∼40 hr orbit. Thus, to the accuracy of ∼1 day, the Na nebula surface brightnesses shown in Figure 4 (top panel) provide a good indicator of the modulations in the escape rate of sodium-bearing material from Io's atmosphere.

The response of the IPT to Io atmospheric escape is somewhat more complicated than that of the Na nebula. The neutral clouds described in the previous paragraph are shaped by interaction with the IPT through the processes of impact ionization and charge-exchange (e.g., Smyth & Marconi, 2003). Impact ionization results in the addition of new material and proceeds on timescales of ∼ 1 day (Smyth & Marconi, 2003). The residence time of plasma in the IPT, is 20 – 80 days, with the shorter residence times corresponding to times of higher total plasma density (Bagenal & Delamere, 2011; Hess et al., 2011; Copper et al., 2016; Tsuchiya et al., 2018). Thus, when there is an enhancement in the escape of sulfur-bearing material from Io's atmosphere, the peak in the IPT S^+ 6731 Å ribbon will lag by an amount dependent on the IPT plasma density. A model is being developed that could, in principle, calculate the precise IPT ribbon response (D. Coffin et al., 2020; D. A. Coffin et al., 2022; D. A. Coffin & Withers, 2023; Nerney & Bagenal, 2020; Nerney et al., 2022, 2023), but its completion and application to the IoIO dataset is beyond the scope of our current project. Thus, we take the ∼4 week delay between the peaks in Na nebula and IPT S^+ emission in the previous two studies that captured contemporaneous enhancements (§5.3; M. E. Brown & Bouchez, 1997; Tsuchiya et al., 2018) as indicative of the plasma transport time during a typical IPT enhancement. Four weeks is also similar to the transport time deduced from the larger IPT enhancement captured by *Cassini* (Steffl et al., 2004; Copper et al., 2016).

6.2 Interpretation of quasi-contemporaneity of Na nebula and IPT enhancements

Within the context of the discussion in Sections 5.3 and 6.1, we can now offer an interpretation the quasi-contemporaneous nature of the Na nebula and IPT enhancements seen in Figure 4. In all cases except 2020, each major Na nebula enhancement has a companion enhancement seen in the IPT nebula that is delayed by ∼4 weeks. This ∼4 week delay is consistent with that seen in previous studies and is indicative of simultaneous release of sodium- and sulfur-bearing material from Io's atmosphere. In 2020, the delay between the Na nebula and IPT enhancements peaks is almost twice as long, however, the profiles of both enhancements are more complicated than the enhancements in other years: the Na nebula enhancement has a shoulder on its trailing edge and the IPT enhancement appears to consist of a broad, main peak, followed by a small, sharp peak. Thus, we offer the suggestion that in mid 2020, there are two overlapping sets of Na nebula and IPT enhancements, with the earlier set being larger than the later. A similar relationship may exist between other, smaller enhancements, such as the shoulder on the early 2020 Na nebula peak and the small IPT peak in mid 2019. We discuss the implications of the variation in the relative Na nebula and IPT peak *sizes* seen in each contemporaneous pair (e.g., fall 2022 being the most extreme) in §6.6.

6.3 Ruling out solar insolation-driven sublimation

The current paradigm holds that the bulk of the escaping material from Io's atmosphere is supplied by Io's global sublimation atmosphere (e.g., Schneider & Bagenal, 2007; Dols et al., 2008, 2012). This paradigm suggests that, in the absence of some other perturbing effect on Io's atmosphere, the variations seen in the Na nebula and IPT should be dominated by variations in solar insolation, that is, Io's 42 hour orbit or Jupiter's 12 year orbit (e.g., de Pater et al., 2020; Tsang et al., 2012). Enhancement in the escape of material from Io's atmosphere may also be modulated by Jupiter's magnetic rotational period (9.925 hr) due to Io's apparent motion within the IPT (e.g., Smyth et al., 2011). Even when considering the timescales of the responses of the Na nebula and IPT to material

escape from Io's atmosphere, discussed in Sections 6.1 – 6.2, solar insolation and magnetic periodicities are not compatible with the behavior of the enhancements seen in Figure 4. Thus, we argue that one or more other physical mechanisms are driving atmospheric escape during enhancements. Since enhancements dominate the average supply of material from Io's atmosphere (Sections 4, 6.1), the process(es) driving enhancements provide the bulk of the material in the Jovian sodium nebula and IPT.

6.4 The case for volcanism

The initial claim of a link between Io volcanism and material release from Io's atmosphere was made using Jovian sodium nebula images recorded with a cadence of weeks to months and disk-integrated infrared observations (Mendillo et al., 2004). A subsequent study using Jovian sodium nebula observations recorded with a near-nightly cadence and a much more extensive set of disk-resolved Io infrared observations, has failed to validate that initial claim (Roth et al., 2020). In this work, we take a different approach and use the time behavior of material release from Io's atmosphere to suggest the most likely driver for atmospheric escape is volcanic plumes.

Recall from §1, that based on EUV brightness of the IPT, $\sim$1 ton s^{-1} of material must be flowing into it from Io's atmosphere. We can now attribute this amount of flux to the mechanism(s) that cause enhancements. Io's atmosphere is itself tenuous and, without resupply from the surface or subsurface, cannot act as a reservoir for supplying enhancements in escape that last weeks to months. We have ruled out variation due to solar insolation-induced sublimation and magnetospherically enhanced escape of Io's global atmosphere, in §6.3. Thus, geologic processes of some sort must ultimately be involved in the dominant process(es) of atmospheric escape from Io's atmosphere.

In §6.2, we showed that enhancements in the escape of sodium and sulfur-bearing material from Io's atmosphere occur simultaneously. This simultaneity, together with the geologic nature of the processes driving escape imply that there is a single geographical location responsible for driving atmospheric escape in each pair of enhancements, with that location not necessarily being the same for each pair. Finally, we note that behavior of the Na nebula and IPT surface brightnesses appears to be stochastic, with large and small enhancements interleaved. The picture that emerges is that geologic activity at discrete sites on Io results in enhancements in the escape of sodium- and sulfur-bearing materials that last 1 – 3 months, with 1 – 2 enhancements seen during each 7 month Jovian opposition observing window and with the relative amount of material escape varying between individual events.

Of the known geologic processes on Io that match the above criteria, volcanism is the most likely to result in the stochastic perturbation of Io's atmosphere, via processes involving plumes. Observational support for Io volcanic plume-driven atmospheric escape comes from the correlation between plumes observed by *Galileo* (P. Geissler et al., 2004; P. E. Geissler & McMillan, 2008) and enhancements in the Jovian dust streams (Krüger, Geissler, et al., 2003). As reviewed in §5.1, the dust streams are composed almost entirely of NaCl and come from Io (Graps et al., 2000; Krüger, Horányi, & Grün, 2003; Postberg et al., 2006). Furthermore, $NaCl^+$ has been shown to be an important pathway for Na escape from Io (Grava et al., 2014; Schmidt et al., 2023). Based on this evidence, it is plausible to suggest that volcanic plumes play a key role in the supply of the Jovian sodium nebula. We use the very large Jovian dust stream enhancement that peaked in early September 2000 and the IPT enhancement observed by *Cassini* that peaked about a month later as observational evidence of the connection between IPT enhancements and volcanic plumes (Krüger, Geissler, et al., 2003; Steffl et al., 2004, see also §5.2).

The difficulty with suggesting that volcanic plumes themselves are responsible for launching material out of Io's atmosphere is that plume vent velocities are far below Io's gravitational escape velocity, even when considering local atmospheric heating by plume

dynamics (e.g., Schneider & Bagenal, 2007; McDoniel et al., 2017; de Pater et al., 2020; Redwing et al., 2022). Thus, if plumes are implicated in material escape from Io, the mechanism must be indirect. Plume models show that shocks in the plume canopy impede upward flow of material, redirecting it outward and toward the surface (Zhang et al., 2003, 2004). Zhang et al. (2003) suggest that the material that is redirected forcibly toward the surface enhances sublimation of SO_2 frost over a large area. Sublimation of SO_2 frosts by hot surface/subsurface lavas would provide a similar localized enhancement in Io's SO_2 atmosphere. This SO_2 would then be available to interact with the IPT via the pathways of sputtering, electron impact ionization and change exchange. The difficulty with this scenario is that it does not provide a comparable mechanism for enhancing the escape of NaCl, since NaCl has a much higher sublimation temperature than SO_2. However, the amount of NaCl provided by the plume itself and/or NaCl lofted from Io's surface by sublimation may be sufficient to drive escape, when considering interaction with the IPT over a large area (see also §6.5).

Perhaps more a more plausible path of escape for both SO_2 and NaX is to consider the ability of plumes to loft material to sufficient altitude to enable enhanced interaction between IPT plasma and the tops of plumes. An extension of the Zhang et al. (2003, 2004) model of Pele's plume shows that by including interaction between the top of the plume and the IPT, better agreement is found with the distribution of material seen on the surface (McDoniel et al., 2015, 2017, 2019). The McDoniel et al. (2019) work provides theoretical validation of the ability of plume tops and IPT plasma to interact, but stops short of a full quantitative calculation of the amount of material that could be removed by this interaction. Thus, although there is observational evidence that connects volcanic plumes to enhancements in the escape of sodium- and sulfur-bearing material from Io's atmosphere, current state-of-the-art theoretical calculations have not been able to determine the exact pathway taken by the material to Io's exosphere.

6.5 Implications for the transport of sodium- and sulfur-bearing material through Io's atmosphere

Atacama Large Millimeter/submillimeter Array (ALMA) observations of Io's atmosphere reveal collections of hot NaCl, KCl and SO_2 gases, that are interpreted as plumes (Redwing et al., 2022). Redwing et al. note that the highest column density collections of alkali and SO_2 gasses are consistently *not* found to be coincident with each other (Figure 9 of that work). As discussed by Redwing et al., these results are difficult to explain given that SO_2, the primary volatile on Io, is expected to be associated with all plume activity. These results are also in apparent conflict with our result that sodium- and sulfur-bearing material are consistently seen to escape at the same time, implying a common geographic source (Sections 6.2 – 6.4). In this Section, we discuss some mechanisms that might contribute to this effect, including those not considered by Redwing et al..

Redwing et al. (2022) provide two potential reasons for the lack of spatial coincidence between alkali and SO_2 plumes in Io's atmosphere which rely on the difference in vaporization pressures of these materials. (1) SO_2 gas is produced primarily by hot lava vaporizing frost deposits, with these deposits found primarily at low- to mid-latitudes. Alkalis sublime at a much higher temperature and therefore will not be released into Io's atmosphere by this effect. (2) The alkalis observed by ALMA are released in the plumes of high-temperature volcanoes. Redwing et al. note that these high-temperature plumes should also produce SO_2 but that these alkali-producing volcanoes are consistently located at high latitudes where atmospheric temperatures may be low enough to freeze SO_2 within the plumes. In this way, (1) explains why SO_2 plumes appear in the absence of alkali plumes (low latitudes) and (2) suggests that SO_2 is always collocated with the high-latitude alkali plumes, however, this high-latitude SO_2 is largely invisible to ALMA because it is in solid form. Evidence of solid-phase transport of SO_2 through Io's atmosphere comes from *Galileo* detection of very high mass-to-charge ratio ions, interpreted as clus-

ters of SO_2 molecules, or "snowflakes," when it flew over Io's north pole (Frank & Paterson, 2002). This explanation requires that the SO_2 gas in the plumes at low latitudes not contribute significantly to SO_2 escape, and requires NaCl to be primarily sourced from the polar plumes, possibly by the mechanism discussed in the next paragraph. Plume models have yet to be constructed that would test this "snowflakes" hypothesis.

Another way to "hide" SO_2 and/or NaCl from ALMA is to ionize them. The behavior of Io's auroral Na, O, SO_2, and SO emission while Io transitions to and from eclipse behind Jupiter provides evidence that (a) photoionization is the primary mechanism for producing SO_2^+ and (b) SO_2^+ plays an important role on the pathway of NaCl escape from Io's atmosphere via charge-exchange (Schmidt et al., 2023). Io's polar atmosphere is exposed to the sun for longer periods of time than that above the rest of Io, thus increasing the average rate of photoionization at the poles. Furthermore, Io's collisional atmosphere is thinner in these regions (e.g., Walker et al., 2010), providing more access of plume material to the exosphere, where IPT-driven escape processes are the most efficient. This suggests that plumes at the poles will have enhanced escape (see also §6.6). Like the SO_2 "snowflake" atmospheric transport mechanism suggested in the previous paragraphs, this mechanism favors the NaCl-rich high-latitude plumes detected by ALMA as the source of the sodium- and sulfur-bearing material contributing to the Na nebula and IPT enhancements.

For logical completeness, we also consider the suggestion that NaCl-containing volcanic dust and ash ("dust bunnies") may transport NaCl through Io's atmosphere in a form not visible to ALMA. To simultaneously explain the ALMA and IoIO data, this would imply that these large particles are driven through the atmosphere by the SO_2 plumes at low latitudes and that those particles are quickly charged by interaction with the IPT and removed from ALMA's FOV by Jupiter's magnetic field. Importantly, under this interpretation, the high-latitude NaCl plumes seen by ALMA would not contribute to escape and the SO_2 from these plumes must still be invisible to ALMA, necessitating one or more of the mechanisms in the previous paragraphs.

In support of the "dust bunny" hypothesis, we recall the observational evidence we used to connect plumes to the Jovian sodium nebula (§6.4; Krüger, Geissler, et al., 2003; Grava et al., 2014; Schmidt et al., 2023). Krüger, Geissler, et al. found that dust stream enhancements were likely associated with the plumes of volcanoes such as Pele, Tvashtar, a region near the north pole, and a region south of Karei (now known as Grian; P. E. Geissler & McMillan, 2008). The plume deposits of these eruptions are primarily SO_2 rich, with minor contributions from silicate ash (P. E. Geissler et al., 1999; P. Geissler et al., 2004). The association between atmospheric escape of sodium- and sulfur-bearing material and these large, SO_2-rich plumes is suggestive that the large atmospheric disturbances caused by these plumes may be the key to driving escape. The lack of association between SO_2-dominated plumes and NaCl emission in the ALMA data then becomes support for transport of NaCl through the atmosphere in these plumes in a form such as dust or ash.

Finally, we suggest that there may be no need to "hide" SO_2 from ALMA in the regions where bright NaCl emission is seen. In the ALMA observation of NaCl and SO_2 that has the highest resolution, relatively faint concentrations of SO_2 gas are seen in the vicinity of the brightest NaCl emission (see 2016-07-26 in Figure 9 of Redwing et al., 2022). More detailed analysis of the ALMA data would be needed to determine if the NaCl and SO_2 seen in this observation is consistent with a single geographic source. Plume models could be used to determine if the amount of SO_2 is, in fact, less than what is expected for the range volcanic activity that has been observed on Io (see, e.g. review by de Pater et al., 2021). Additional high-resolution ALMA images, ideally recorded contemporaneously with IoIO data, would also be useful. If the NaCl to SO_2 ratio were to be found to be reasonable in NaCl plumes, this could imply that atmospheric escape is primarily tied to NaCl-rich and/or high-latitude plumes and that the collections of high col-

umn density SO_2 gas seen at lower latitudes in the ALMA data contribute at most a minor, steady amount to the IPT (e.g., baseline in Figure 4, bottom panel.)

6.6 Processes that modulate Na nebula and IPT enhancement sizes

Having established that volcanic plumes are the likely precipitating agent for material escape from Io's atmosphere and discussed possible pathways of material transport through Io's atmosphere, we return to our discussion of the quasi-contemporaneous nature of the Na nebula and IPT enhancements, begun in §6.2, to offer possible causes for the modulation seen in the *sizes* of Na nebula and IPT enhancements. These suggested causes divide into four general categories: (1) variation in the content of sodium- and sulfur-bearing material in volcanic plumes, such as produced by different magmas (e.g., see Redwing et al., 2022); (2) processes involving the interaction of the plumes with the atmosphere, such as shocks (§6.4; Zhang et al., 2003, 2004) (3) modulation in material transport through the atmosphere (§6.5; Schmidt et al., 2023); and (4) variation in the efficiency of escape. In this Section, we concentrate on category (4), because understanding effects in this category greatly enhances the ability to use Jovian sodium nebula and IPT data to make progress understanding physical effects in categories (1) – (3).

One of the scenarios discussed in §6.5 suggested that enhanced SO_2 ionization in Io's polar regions may play a role in enhancing NaCl escape (Schmidt et al., 2023). This would favor the Tvashtar plume (63°N 124°W) over that of Pele (19°S 255°W) or Surt (45°N, 336°W) for the source of the very large Jovian dust stream enhancement observed by *Galileo* in late 2000, even though Surt, active at the time, had a much larger infrared output and Pele was the most active large plume during the *Galileo* era (Marchis et al., 2002; Porco et al., 2003; Krüger, Geissler, et al., 2003; P. Geissler et al., 2004). Because SO_2 ionization and subsequent rapid dissociation (Huddleston et al., 1998) may be enhanced in the polar regions (Schmidt et al., 2023), the efficiency of S and O production, and thus escape, may be enhanced at the poles as well.

Because $NaCl^+$ has an important role in the pathway of Na escape from Io's atmosphere (Sections 5.1, 6.4, 6.5; Schmidt et al., 2023), sodium-bearing material in Io's anti-Jovian equatorial exosphere may have an exaggerated escape efficiency over that of sulfur-bearing material. The sodium "jet" was seen to be rooted in the anti-Jovian equatorial region of Io's exosphere the one time it has been imaged in sufficient spatial detail for detection near Io (Burger et al., 1999). Burger et al. offered two hypotheses to explain this behavior: (i) Material was being injected into the exosphere from below at this location, e.g., by volcanism. (ii) Ionization is enhanced in this region due to Io equatorial auroral activity (e.g., Roesler et al., 1999; P. E. Geissler et al., 1999; Roth et al., 2014). Case (ii) would provide a mechanism for enhancing material flow into the jet, over material flow to the IPT, since the jet is formed by prompt neutralization of pickup ions within Io's exosphere (Schneider et al., 1991; Wilson & Schneider, 1994), whereas direct ionization of material in Io's exosphere has been shown to be a minor contributor to the influx of plasma to the IPT (§1; Dols et al., 2008, 2012). The prompt neutralization of the sodium forming the jet also explains why it is not expected to be seen rooted at the sub-Jovian auroral spot: the initial gyration of the ions directs them into Io's surface. We note that hypotheses (i) and (ii) are not necessarily mutually exclusive: the "jet" may always be rooted in the region of the anti-Jovian equatorial auroral spot, but its response to atmospheric escape may be exaggerated if that atmospheric escape is located in that region.

Finally, dust, which acquires a negative charge (Zook et al., 1996), enhances the initial escape of Na-bearing material on Io's sub-Jovian hemisphere (Grava et al., 2021). As the dust particles are destroyed and the constituent molecules and atoms are released, they acquire a positive charge and join the "jet" feature. A positive identification be-

tween a Na nebula enhancement and a plume on the sub-Jovian hemisphere, could thus potentially be used in support of the "dust bunnies" hypothesis discussed in §6.5.

6.7 Toward a connection with Io infrared observations

Since the early 1980s, synoptic Io infrared observations have been used to help understand Io volcanic processes and their geologic implications (e.g., see review by de Pater et al., 2021). As noted in §6.4, these infrared observations have been compared to sodium nebula observations in an attempt to establish a correlation (Mendillo et al., 2004) which has not stood the test of time (Roth et al., 2020). The initial attempt to connect infrared indicators of Io volcanic activity to enhancements in the sodium nebula made the implicit assumption that the brightest infrared events should be correlated to the brightest nebula images. Here we suggest that instead, the dimmer infrared events may be more likely to be correlated to the brighter sodium nebula enhancements.

One of the fundamental results of our study is that the Jovian sodium nebula and IPT show contemporaneous enhancements of varying relative amplitudes that last 1 – 3 months (Figure 4; Sections 4, 6.1 – 6.2). A long-term study of the time variability of Io's hotspots found that they divided into two groups: those with persistent activity and those that exhibited sudden brightening, followed by a steady decay (de Kleer & de Pater, 2016). For those hotspots that exhibited sudden brightening events, the brighter the event, the shorter the decay (see, e.g., Figure 11 of de Kleer & de Pater, 2016). The hot spots with decay times of order 1 month or longer were dimmer, by a factor of 5 or more, than the brightest outbursts. If we make the very simplistic assumption that in a volcano where plume activity is found, plume activity will persist over roughly the same time period as infrared activity, we can support the argument that infrared hotspots exhibiting eruption phases lasting 1 – 3 months are the more likely to be correlated to atmospheric release events. Thus, dim infrared outbursts may be the most likely to be correlated with enhancements in material release from Io's atmosphere.

7 Summary and Conclusions

We have used IoIO, an observatory composed almost entirely off-the-shelf equipment (§2 and Morgenthaler et al., 2019) to collect the largest set of contemporaneously recorded Jovian sodium nebula and Io plasma torus (IPT) in [S II] 6731 Å images assembled to date (see examples in Figure 1 and accompanying animations). Using simple image analysis techniques (§3), we construct a time history of the brightnesses of the Na nebula and IPT [S II] emission (Figure 4). Qualitative inspection of this Figure shows 1 – 2 enhancements in the Na nebula and IPT [S II] emission per ∼7-month observing window, such that a quiescent state of emission is rare (§4). The minimum and maximum surface brightness values seen in the IoIO Na nebula and IPT images compare favorably with previous studies (§5.1 – 5.2). Most large IPT enhancements peak ∼4-weeks after the corresponding enhancement in the Na nebula, as seen in previous studies (§5.3) and as expected from plasma transport within the IPT (§6.1). The exception to this, seen in mid 2020, is likely caused by the overlap of multiple enhancements (§6.2). We rule out sublimation as the primary driver of material escape from Io's atmosphere in §6.3. This is our most definitive result.

Having ruled out sublimation as the primary driver of atmospheric escape from Io, we show that geologic activity in some form, likely volcanic plumes, drives escape, either directly or indirectly (§6.4). In light of other published results, this has implications on the transport of material through Io's atmosphere (§6.5). In §6.6, we review the processes that can modulate the relative sizes of contemporaneous Na nebula and IPT enhancements, focusing on processes that might modulate the efficiency of Io atmospheric escape as a function of geographic location. Finally, in §6.7, we note that Io's dimmer infrared outbursts have durations and time profiles similar to Na nebula and IPT enhance-

ments, suggesting that it these 1 – 3 month-long infrared outbursts may be the more likely to show correlation with the release of material from Io's atmosphere.

In conclusion, our work shows that off-the-shelf equipment with minimal customization, together with simple analysis techniques can be used to collect data that provides valuable insights into the processes which produce material on Io's surface, transport it through its atmosphere, and release it into Jupiter's broader magnetospheric environment.

8 Future Plans

We have pointed out the existing observational evidence that links plume activity on Io to atmospheric escape in §6.4. Further confirmation of this link may be accomplished by accumulating additional contemporaneous IoIO observations of the Na nebula and IPT together with ALMA observations of Io's atmosphere – currently there is only overlap during March 2018 (Redwing et al., 2022). Disk-integrated observations conducted by the NOrthern Extended Millimetre Array (NOEMA) interferometer of the Institut de Radioastronomie Millimetrique (IRAM), such as those conducted by Roth et al. (2020), may also be useful. Continued theoretical work on the effect that plumes have on Io's atmosphere and exosphere, as well as the interaction between the exosphere and the IPT is also needed (e.g., Blöcker et al., 2018; McDoniel et al., 2019; Dols et al., 2008, 2012; Dols & Johnson, 2023; Adeloye et al., 2023). These observational and theoretical studies can also be useful to help differentiate between the hypotheses offered in 6.5 concerning material transport through Io's atmosphere.

Continued disk-resolved observations of Io IR activity, such as those carried out at the Keck and Gemini telescopes (de Kleer et al., 2019) will also be interesting as they might lead to validation of the correlation that was initially claimed between Na nebula, IPT and IR brightnesses (Mendillo et al., 2004; Yoshikawa et al., 2017; Yoshioka et al., 2018; Tao et al., 2018; Koga et al., 2018b), but has subsequently proven elusive (de Kleer et al., 2016; Roth et al., 2020).

We are also planning to conduct more detailed analysis of the IoIO images. For instance, the IoIO images of the Na nebula contain three distinct features – the "banana," "jet," and "stream" – that can be used to estimate the neutral sodium source rate from Io (Wilson et al., 2002). The IPT ribbon positions, which are detectable with IoIO (Figure 3, lower panels), are related to the dawn-dusk electric field, which is modulated by a combination of material flow toward the magnetotail and solar wind pressure (Barbosa & Kivelson, 1983; Ip & Goertz, 1983). When combined with the analysis presented here, the IPT ribbon positions retrieved from the IoIO data will provide a significant amount of information regarding the production of material on Io and its subsequent flow through and out of Jupiter's magnetosphere.

Finally, the unique sensitivity of IoIO to Na nebula and IPT [S II] 6731 Å enhancements, together with reliable robotic operation and <24 hour turnaround for pipeline reduction ideally suits it to provide real-time alerts of enhancements in the departure of material from Io's atmosphere. These can inform planned observations of Io from both ground- and space-based platforms. In particular, nearly all of the plasma found in Jupiter's magnetosphere comes from Io and makes its way through the IPT in 20 – 80 days before rapidly spiraling out through the rest of the magnetosphere (Bagenal & Delamere, 2011; Hess et al., 2011; Copper et al., 2016; Tsuchiya et al., 2018). The modulations seen in the lower panel of Figure 4 therefore precede modulation in plasma density throughout the Jovian magnetosphere, a feature that can be used to enhance the science operations of the *Juno* mission (Bolton et al., 2017) and supporting observations (Orton et al., 2020, 2022). NASA's *Europa Clipper* (Howell & Pappalardo, 2020) and ESA's *JUICE* (Grasset et al., 2013) missions will benefit from planned IoIO observations, because of

the record of exogenic material impinging on Europa, Ganymede and Callisto during those missions. Also, because enhancements in the Jovian dust streams can induce detector fatigue in *Europa Clipper's* SUrface Dust Analyzer (SUDA; Goode et al., 2023), IoIO observations can be used to inform SUDA operations while *Europa Clipper* is sampling the broader Jovian magnetospheric environment and thus optimize detector performance for that mission's primary target.

Open Research Section

The following software was used in this project: Astrometry.net (Lang et al., 2010), AstroPy (Astropy Collaboration et al., 2022), Astroquery (Ginsburg et al., 2019), BigMultiPipe (Morgenthaler, 2022), Burnashev (Morgenthaler, 2023b), CCDMultiPipe (Morgenthaler, 2023c), ccdproc (Craig et al., 2017), IoIO control software (Morgenthaler, 2023a), matplotlib (Hunter, 2007), moviepy (Zulko et al., 2021), NumPy (Oliphant, 2006; Harris et al., 2020), photutils (Bradley et al., 2022), precisionguide (Morgenthaler, 2023d), Python 3 (Van Rossum & Drake, 2009), reproject (Robitaille et al., 2020), SciPy (Virtanen et al., 2020), specutils (Earl et al., 2022)

The reduction products used to create Figure 4 are archived with Zenodo (Morgenthaler et al., 2023).

Acknowledgments

IoIO is hosted at the San Pedro Valley Observatory, near Benson, Arizona, and has benefited greatly from the services provided by observatory manager, Dean Salman. Gavin Nelson, Andy Sorenson, Elisabeth Adams, and the staff of Starizona have also provided invaluable assistance in observatory maintenance. The authors are grateful for the insightful comments received during the manuscript review process. This work has been supported by NSF grants 1616928 and 2109219 and NASA grant 80NSSC22K0317 to the Planetary Science Institute and NASA grant 80NSSC20K0559 to Boston University.

References

Adams, E., Jackson, B., Sickafoose, A., Morgenthaler, J., Stubbers, H., Carson, D., & Worters, H. (2023). Finding doomed worlds: searching for ultra-hot jupiters with decaying orbits. *Bull. Am. Astron. Soc.*, *55*, 403.05.

Adeloye, A., Trafton, L., Goldstein, D., Varghese, P., & Mahieux, A. (2023, October). Investigating Io's Tvashtar Plume: DSMC Simulations, Mie Theory Analysis, and Implications for Entrained Particulate Properties. *Bull. Am. Astron. Soc.*, *55*, 111.03.

Astropy Collaboration, Price-Whelan, A. M., Lim, P. L., Earl, N., Starkman, N., Bradley, L., ... Astropy Project Contributors (2022, August). The Astropy Project: Sustaining and Growing a Community-oriented Open-source Project and the Latest Major Release (v5.0) of the Core Package. *Astrophys. J.*, *935*(2), 167. doi: 10.3847/1538-4357/ac7c74

Bagenal, F., & Delamere, P. A. (2011, May). Flow of mass and energy in the magnetospheres of Jupiter and Saturn. *JGR: Space Physics*, *116*, A05209. doi: 10.1029/2010JA016294

Barbosa, D. D., & Kivelson, M. G. (1983, March). Dawn-dusk electric field asymmetry of the Io plasma torus. *Geophys. Res. Lett.*, *10*(3), 210-213. doi: 10.1029/GL010i003p00210

Beers, T. C., Flynn, K., & Gebhardt, K. (1990, July). Measures of Location and Scale for Velocities in Clusters of Galaxies—A Robust Approach. *AJ*, *100*, 32. doi: 10.1086/115487

Blöcker, A., Saur, J., Roth, L., & Strobel, D. F. (2018, Nov). MHD Modeling of the

Plasma Interaction With Io's Asymmetric Atmosphere. *JGR: Space Physics*, *123*(11), 9286-9311. doi: 10.1029/2018JA025747

Bolton, S. J., Lunine, J., Stevenson, D., Connerney, J. E. P., Levin, S., Owen, T. C., ... Thorpe, R. (2017, November). The Juno Mission. *Space Sci. Rev.*, *213*(1-4), 5-37. doi: 10.1007/s11214-017-0429-6

Bradley, L., Sipöcz, B., Robitaille, T., Tollerud, E., Vinícius, Z., Deil, C., ... Souchereau, H. (2022, July). *astropy/photutils: 1.5.0* [Computer Software]. Zenodo. doi: 10.5281/zenodo.6825092

Broadfoot, A. L., Belton, M. J., Takacs, P. Z., Sandel, B. R., Shemansky, D. E., Holberg, J. B., ... McElroy, M. B. (1979, June). Extreme ultraviolet observations from voyager 1 encounter with jupiter. *Sci*, *204*, 979-982. doi: 10.1126/science.204.4396.979

Brown, M. E. (1994). *The Structure and Variability of the Io Plasma Torus* (Unpublished doctoral dissertation). University of California, Berkeley.

Brown, M. E., & Bouchez, A. H. (1997, October). The response of Jupiter's magnetosphere to an outburst on Io. *Sci*, *278*, 268-271. doi: 10.1126/science.278.5336.268

Brown, R. A., & Chaffee, F. H., Jr. (1974, February). High-Resolution Spectra of Sodium Emission from Io. *Astrophys. J., Lett.*, *187*, L125. doi: 10.1086/181413

Burger, M. H., Schneider, N. M., & Wilson, J. K. (1999, November). Galileo's close-up view of the Io sodium jet. *Geophys. Res. Lett.*, *26*(22), 3333-3336. doi: 10.1029/1999GL003654

Burnashev, V. I. (1985, January). Catalogue of data on energy distribution in spectra of stars in a uniform spectrophotometric system. *Abastumanskaia Astrofizicheskaia Observatoriia Byulleten*, *59*, 83-89.

Coffin, D., Delamere, P., & Damiano, P. (2020, May). Implications for Magnetosphere-Ionosphere Coupling From Jupiter's System IV Quasi-Period. *JGR: Space Physics*, *125*(5), e27347. doi: 10.1029/2019JA027347

Coffin, D. A., Delamere, P. A., Bagenal, F., & Nerney, E. G. (2022). Examining the Europa plasma environment via a multi-dimensional physical chemistry model. *AGU Fall Meeting Abstracts*, *2022*, SM55B-1457.

Coffin, D. A., & Withers, P. (2023). The Consequences of Alfvénic Inefficiency in Coupling Jupiter with the Io Plasma Torus. *AGU Fall Meeting Abstracts*, *2023*, SM23D-2845.

Connerney, J. E. P., Acuña, M. H., Ness, N. F., & Satoh, T. (1998, June). New models of Jupiter's magnetic field constrained by the Io flux tube footprint. *JGR: Space Physics*, *103*(A6), 11929-11940. doi: 10.1029/97JA03726

Connerney, J. E. P., Kotsiaros, S., Oliversen, R. J., Espley, J. R., Jørgensen, J. L., Jørgensen, P. S., ... Levin, S. M. (2018, March). A New Model of Jupiter's Magnetic Field From Juno's First Nine Orbits. *Geophys. Res. Lett.*, *45*(6), 2590-2596. doi: 10.1002/2018GL077312

Copper, M., Delamere, P. A., & Overcast-Howe, K. (2016, July). Modeling physical chemistry of the Io plasma torus in two dimensions. *JGR: Space Physics*, *121*(7), 6602-6619. doi: 10.1002/2016JA022767

Craig, M., Crawford, S., Seifert, M., Robitaille, T., Sipőcz, B., Walawender, J., ... Streicher, O. (2017, December). *astropy/ccdproc: v1.3.0.post1* [Computer Software]. Zenodo. doi: 10.5281/zenodo.1069648

de Kleer, K., & de Pater, I. (2016, December). Time variability of Io's volcanic activity from near-IR adaptive optics observations on 100 nights in 2013-2015. *Icarus*, *280*, 378-404. doi: 10.1016/j.icarus.2016.06.019

de Kleer, K., de Pater, I., Molter, E. M., Banks, E., Davies, A. G., Alvarez, C., ... Tollefson, J. (2019, July). Io's Volcanic Activity from Time Domain Adaptive Optics Observations: 2013-2018. *AJ*, *158*(1), 29. doi: 10.3847/1538-3881/ab2380

de Kleer, K., de Pater, I., & Yoneda, M. (2016, December). Io's Volcanic Activity in 2013-2016 and Comparison with Extended Sodium Cloud Variability. *AGU Fall Meeting Abstracts*, P21E-04. (presented at 2016 Fall Meeting, AGU, San Francisco, Calif., 12-16 Dec.)

de Pater, I., Keane, J. T., de Kleer, K., & Davies, A. G. (2021, May). A 2020 Observational Perspective of Io. *Annual Review of Earth and Planetary Sciences*, *49*. doi: 10.1146/annurev-earth-082420-095244

de Pater, I., Luszcz-Cook, S., Rojo, P., Redwing, E., de Kleer, K., & Moullet, A. (2020, December). ALMA Observations of Io Going into and Coming out of Eclipse. *Planetary Sci. J.*, *1*(3), 60. doi: 10.3847/PSJ/abb93d

Dols, V., Delamere, P. A., & Bagenal, F. (2008, September). A multispecies chemistry model of Io's local interaction with the Plasma Torus. *Journal of Geophysical Research (Space Physics)*, *113*(A9), A09208. doi: 10.1029/2007JA012805

Dols, V., Delamere, P. A., Bagenal, F., Kurth, W. S., & Paterson, W. R. (2012, October). Asymmetry of Io's outer atmosphere: Constraints from five Galileo flybys. *JGR: Planets*, *117*(E16), E10010. doi: 10.1029/2012JE004076

Dols, V., & Johnson, R. E. (2023, March). Ion-molecule charge exchange in Io's extended atmosphere: Velocity dependence. *Icarus*, *392*, 115365. doi: 10.1016/j.icarus.2022.115365

Earl, N., Tollerud, E., Jones, C., O'Steen, R., Kerzendorf, W., Busko, I., ... Ferguson, H. (2022, February). *astropy/specutils* [Computer Software]. Zenodo. Retrieved from `https://doi.org/10.5281/zenodo.1421356` doi: 10.5281/zenodo.1421356

Frank, L. A., & Paterson, W. R. (2002, August). Plasmas observed with the Galileo spacecraft during its flyby over Io's northern polar region. *Journal of Geophysical Research (Space Physics)*, *107*(A8), 1220. doi: 10.1029/2002JA009240

Geissler, P., McEwen, A., Phillips, C., Keszthelyi, L., & Spencer, J. (2004, May). Surface changes on Io during the Galileo mission. *Icarus*, *169*(1), 29-64. doi: 10.1016/j.icarus.2003.09.024

Geissler, P. E., McEwen, A. S., Ip, W., Belton, M. J. S., Johnson, T. V., Smyth, W. H., & Ingersoll, A. P. (1999, August). Galileo Imaging of Atmospheric Emissions from Io. *Sci*, *285*, 870-874. doi: 10.1126/science.285.5429.870

Geissler, P. E., & McMillan, M. T. (2008, Oct). Galileo observations of volcanic plumes on Io. *Icarus*, *197*(2), 505-518. doi: 10.1016/j.icarus.2008.05.005

Ginsburg, A., Sipőcz, B. M., Brasseur, C. E., Cowperthwaite, P. S., Craig, M. W., Deil, C., ... a subset of the astropy collaboration (2019, March). astroquery: An Astronomical Web-querying Package in Python. *AJ*, *157*, 98. doi: 10.3847/1538-3881/aafc33

Giorgini, J. D., Yeomans, D. K., Chamberlin, A. B., Chodas, P. W., Jacobson, R. A., Keesey, M. S., ... Wimberly, R. N. (1996, September). JPL's On-Line Solar System Data Service. *Bull. Am. Astron. Soc.*, *28*, 25.04.

Goode, W., Kempf, S., & Schmidt, J. (2023, March). Mapping the surface composition of Europa with SUDA. *Planet. Space Sci.*, *227*, 105633. doi: 10.1016/j.pss.2023.105633

Graps, A. L., Grün, E., Svedhem, H., Krüger, H., Horányi, M., Heck, A., & Lammers, S. (2000, May). Io as a source of the jovian dust streams. *Nature*, *405*(6782), 48-50. doi: 10.1038/35011008

Grasset, O., Dougherty, M. K., Coustenis, A., Bunce, E. J., Erd, C., Titov, D., ... Van Hoolst, T. (2013, April). JUpiter ICy moons Explorer (JUICE): An ESA mission to orbit Ganymede and to characterise the Jupiter system. *Planet. Space Sci.*, *78*, 1-21. doi: 10.1016/j.pss.2012.12.002

Grava, C., Cassidy, T. A., Schneider, N. M., Hsu, H.-W., Morgenthaler, J. P., Leblanc, F., ... Barbieri, C. (2021, November). A Possible Dust Origin for an Unusual Feature in Io's Sodium Neutral Clouds. *AJ*, *162*(5), 190. doi:

10.3847/1538-3881/ac1ff8

Grava, C., Schneider, N. M., Leblanc, F., Morgenthaler, J. P., Mangano, V., & Barbieri, C. (2014, March). Solar control of sodium escape from Io. *Journal of Geophysical Research (Planets)*, *119*, 404-415. doi: 10.1002/2013JE004504

Harris, C. R., Millman, K. J., van der Walt, S. J., Gommers, R., Virtanen, P., Cournapeau, D., ... Oliphant, T. E. (2020, September). Array programming with NumPy. *Nature*, *585*(7825), 357–362. doi: 10.1038/s41586-020-2649-2

Herbert, F., Schneider, N. M., & Dessler, A. J. (2008, Jan). New description of Io's cold plasma torus. *JGR: Space Physics*, *113*(A1), A01208. doi: 10.1029/2007JA012555

Hess, S. L. G., Delamere, P. A., Bagenal, F., Schneider, N., & Steffl, A. J. (2011, November). Longitudinal modulation of hot electrons in the Io plasma torus. *JGR: Space Physics*, *116*(A15), 11215. doi: 10.1029/2011JA016918

Hikida, R., Yoshioka, K., Murakami, G., Kimura, T., Tsuchiya, F., Yamazaki, A., ... Iwagami, N. (2018, July). Identification of Extreme Ultraviolet Emission Lines of the Io Plasma Torus Observed by Hisaki/EXCEED. *Journal of Geophysical Research (Planets)*, *123*(7), 1723-1731. doi: 10.1029/2018JE005629

Hikida, R., Yoshioka, K., Tsuchiya, F., Kagitani, M., Kimura, T., Bagenal, F., ... Yoshikawa, I. (2020, March). Spatially Asymmetric Increase in Hot Electron Fraction in the Io Plasma Torus During Volcanically Active Period Revealed by Observations by Hisaki/EXCEED From November 2014 to May 2015. *JGR: Space Physics*, *125*(3), e27100. doi: 10.1029/2019JA027100

Howell, S. M., & Pappalardo, R. T. (2020, March). NASA's Europa Clipper—a mission to a potentially habitable ocean world. *Nature Communications*, *11*, 1311. doi: 10.1038/s41467-020-15160-9

Huddleston, D. E., Strangeway, R. J., Warnecke, J., Russell, C. T., & Kivelson, M. G. (1998, September). Ion cyclotron waves in the Io torus: Wave dispersion, free energy analysis, and SO_2^+ source rate estimates. *J. Geophys. Res.*, *103*(E9), 19887-19900. doi: 10.1029/97JE03557

Hunter, J. D. (2007). Matplotlib: A 2d graphics environment. *Computing In Science & Engineering*, *9*(3), 90–95. doi: 10.1109/MCSE.2007.55

Ip, W.-H., & Goertz, C. K. (1983, March). An interpretation of the dawn-dusk asymmetry of UV emission from the Io plasma torus. *Nature*, *302*, 232. doi: 10.1038/302232a0

Jockers, K., Thomas, N., Bonev, T., Ivanova, V., & Shkodrov, V. (1992, August). Observations of Io's sodium cloud and torus. *Advances in Space Research*, *12*(8), 347-351. doi: 10.1016/0273-1177(92)90409-Q

Kagitani, M., Sakanoi, T., Kasaba, Y., & Okano, S. (2020, December). A coronagraph using a digital micromirror device as an adaptive occultation mask: design and observational result. *Proceedings of SPIE*, *11447*, 114479Y. doi: 10.1117/12.2561906

Kimura, T., Hiraki, Y., Tao, C., Tsuchiya, F., Delamere, P. A., Yoshioka, K., ... Fujimoto, M. (2018, March). Response of Jupiter's Aurora to Plasma Mass Loading Rate Monitored by the Hisaki Satellite During Volcanic Eruptions at Io. *JGR: Space Physics*, *123*, 1885-1899. doi: 10.1002/2017JA025029

Koga, R., Tsuchiya, F., Kagitani, M., Sakanoi, T., Yoneda, M., Yoshioka, K., ... Bagenal, F. (2018a, May). Spatial Distribution of Io's Neutral Oxygen Cloud Observed by Hisaki. *JGR: Space Physics*, *123*, 3764-3776. doi: 10.1029/2018JA025328

Koga, R., Tsuchiya, F., Kagitani, M., Sakanoi, T., Yoneda, M., Yoshioka, K., ... Smith, H. T. (2018b, January). The time variation of atomic oxygen emission around Io during a volcanic event observed with Hisaki/EXCEED. *Icarus*, *299*, 300-307. doi: 10.1016/j.icarus.2017.07.024

Krüger, H., Geissler, P., Horányi, M., Graps, A. L., Kempf, S., Srama, R., ... Grün, E. (2003, November). Jovian dust streams: A monitor of Io's volcanic plume

activity. *Geophys. Res. Lett.*, *30*(21), 210000-1. doi: 10.1029/2003GL017827

Krüger, H., Horányi, M., & Grün, E. (2003, January). Jovian dust streams: Probes of the Io plasma torus. *Geophys. Res. Lett.*, *30*(2), 1058. doi: 10.1029/2002GL015920

Kumar, S. (1979, August). The stability of an SO_2 atmosphere on Io. *Nature*, *280*(5725), 758-760. doi: 10.1038/280758a0

Kupo, I., Mekler, Y., & Eviatar, A. (1976, April). Detection of ionized sulfur in the Jovian magnetosphere. *Astrophys. J., Lett.*, *205*, L51-L53. doi: 10.1086/182088

Lang, D., Hogg, D. W., Mierle, K., Blanton, M., & Roweis, S. (2010, May). Astrometry.net: Blind Astrometric Calibration of Arbitrary Astronomical Images. *AJ*, *139*(5), 1782-1800. doi: 10.1088/0004-6256/139/5/178210.48550/arXiv.0910.2233

Lellouch, E., Paubert, G., Moses, J. I., Schneider, N. M., & Strobel, D. F. (2003, January). Volcanically emitted sodium chloride as a source for io's neutral clouds and plasma torus. *Nature*, *421*, 45-47. doi: 10.1038/nature01292

Marchis, F., de Pater, I., Davies, A. G., Roe, H. G., Fusco, T., Le Mignant, D., ... Prangé, R. (2002, November). High-Resolution Keck Adaptive Optics Imaging of Violent Volcanic Activity on Io. *Icarus*, *160*(1), 124-131. doi: 10.1006/icar.2002.6955

McDoniel, W. J., Goldstein, D. B., Varghese, P. L., & Trafton, L. M. (2015, September). Three-dimensional simulation of gas and dust in Io's Pele plume. *Icarus*, *257*, 251-274. doi: 10.1016/j.icarus.2015.03.019

McDoniel, W. J., Goldstein, D. B., Varghese, P. L., & Trafton, L. M. (2017, September). The interaction of Io's plumes and sublimation atmosphere. *Icarus*, *294*, 81-97. doi: 10.1016/j.icarus.2017.04.021

McDoniel, W. J., Goldstein, D. B., Varghese, P. L., & Trafton, L. M. (2019, July). Simulation of Io's plumes and Jupiter's plasma torus. *Physics of Fluids*, *31*(7), 077103. doi: 10.1063/1.5097961

McGrath, M. A., & Johnson, R. E. (1987, March). Magnetospheric plasma sputtering of Io's atmosphere. *Icarus*, *69*(3), 519-531. doi: 10.1016/0019-1035(87)90021-2

McGrath, M. A., Lellouch, E., Strobel, D. F., Feldman, P. D., & Johnson, R. E. (2004). Satellite atmospheres. In F. Bagenal, T. E. Dowling, & W. B. McKinnon (Eds.), *Jupiter. the planet, satellites and magnetosphere* (p. 457-483). Cambridge: Cambridge University Press.

Mendillo, M., Baumgardner, J., Flynn, B., & Hughes, W. J. (1990, November). The extended sodium nebula of Jupiter. *Nature*, *348*, 312-314. doi: 10.1038/348312a0

Mendillo, M., Wilson, J., Spencer, J., & Stansberry, J. (2004, August). Io's volcanic control of Jupiter's extended neutral clouds. *Icarus*, *170*, 430-442. doi: 10.1016/j.icarus.2004.03.009

Moirano, A., Gomez Casajus, L., Zannoni, M., Durante, D., & Tortora, P. (2021, October). Morphology of the Io Plasma Torus From Juno Radio Occultations. *Journal of Geophysical Research (Space Physics)*, *126*(10), e29190. doi: 10.1029/2021JA029190

Morabito, L. A., Synnott, S. P., Kupferman, P. N., & Collins, S. A. (1979, June). Discovery of currently active extraterrestrial volcanism. *Sci*, *204*, 972. doi: 10.1126/science.204.4396.972

Morgan, J. S. (1985, June). Temporal and spatial variations in the Io torus. *Icarus*, *62*, 389-414. doi: 10.1016/0019-1035(85)90183-6

Morgenthaler, J. P. (2022, December). *jpmorgen/bigmultipipe* [Computer Software]. Zenodo. doi: 10.5281/zenodo.7485043

Morgenthaler, J. P. (2023a, January). *Io Input/Output facility (IoIO) control, reduction, and analysis software* [Computer Software]. Zenodo. doi: 10.5281/zenodo

.834711710.5281/zenodo.7703222

Morgenthaler, J. P. (2023b, January). *jpmorgen/burnashev* [Computer Software]. Zenodo. doi: 10.5281/zenodo.7507994

Morgenthaler, J. P. (2023c, January). *jpmorgen/ccdmultipipe* [Computer Software]. Zenodo. doi: 10.5281/zenodo.7507738

Morgenthaler, J. P. (2023d, January). *jpmorgen/precisionguide* [Computer Software]. Zenodo. doi: 10.5281/zenodo.7507157

Morgenthaler, J. P., Rathbun, J. A., Schmidt, C. A., Baumgardner, J., & Schneider, N. M. (2019, jan). Large volcanic event on io inferred from jovian sodium nebula brightening. *Astrophys. J., Lett.*, *871*(2), L23. doi: 10.3847/2041-8213/aafdb7

Morgenthaler, J. P., Schmidt, C. A., Vogt, M., Schneider, N. M., & Marconi, M. (2023, September). *Io Input/Output observatory (IoIO) reduction products.* Zenodo. Retrieved from `https://doi.org/10.5281/zenodo.8342758` doi: 10.5281/zenodo.8342758

Moullet, A., Gurwell, M. A., Lellouch, E., & Moreno, R. (2010, July). Simultaneous mapping of SO_2, SO, NaCl in Io's atmosphere with the Submillimeter Array. *Icarus*, *208*(1), 353-365. doi: 10.1016/j.icarus.2010.02.009

Nerney, E. G., & Bagenal, F. (2020, April). Combining UV Spectra and Physical Chemistry to Constrain the Hot Electron Fraction in the Io Plasma Torus. *JGR: Space Physics*, *125*(4), e27458. doi: 10.1029/2019JA027458

Nerney, E. G., Bagenal, F., Coffin, D. A., & Delamere, P. A. (2022, December). 3D Physical Chemistry and Emission Simulations of the Io Plasma Torus. In *Agu fall meeting abstracts* (Vol. 2022, p. SM55B-1456).

Nerney, E. G., Bagenal, F., & Schmidt, C. (2023, October). A 3D Model of the Io Plasma torus and Model Comparisons with Observations. *Bull. Am. Astron. Soc.*, *55*, 111.05.

Nozawa, H., Misawa, H., Takahashi, S., Morioka, A., Okano, S., & Sood, R. (2004, July). Long-term variability of [S II] emissions from the Io plasma torus between 1997 and 2000. *JGR: Space Physics*, *109*, 7209. doi: 10.1029/2003JA010241

Oliphant, T. E. (2006). *Guide to NumPy*. Provo: Trelgol Publishing.

Oliversen, R. J., Scherb, F., & Roesler, F. L. (1991, September). The io sulfur torus in 1981. *Icarus*, *93*, 53–62.

Orton, G., Momary, T., Brueshaber, S., Hansen, C., Bolton, S., & Rogers, J. (2022, September). The Juno Extended Mission: A Call for Continued Support from Amateur Observers. In *European planetary science congress* (p. EPSC2022-769). doi: 10.5194/epsc2022-769

Orton, G., Tabataba-Vakili, F., & Momary, T. (2020, March). The Earth-Based Observational Program for Juno Mission Support. In *Planets 2020, ground and space observatories: a joint venture to planetary science* (p. 17). doi: 10.5281/zenodo.4435595

Pearl, J., Hanel, R., Kunde, V., Maguire, W., Fox, K., Gupta, S., ... Raulin, F. (1979, August). Identification of gaseous SO_2 and new upper limits for other gases on Io. *Nature*, *280*(5725), 755-758. doi: 10.1038/280755a0

Phipps, P. H., & Bagenal, F. (2021, January). Centrifugal Equator in Jupiter's Plasma Sheet. *Journal of Geophysical Research (Space Physics)*, *126*(1), e28713. doi: 10.1029/2020JA028713

Pilcher, C. B., Fertel, J. H., Smyth, W. H., & Combi, M. R. (1984, December). Io's sodium directional features - Evidence for a magnetospheric-wind-driven gas escape mechanism. *Astrophys. J.*, *287*, 427-444. doi: 10.1086/162702

Plane, J. M. C., Flynn, G. J., Määttänen, A., Moores, J. E., Poppe, A. R., Carrillo-Sanchez, J. D., & Listowski, C. (2018, February). Impacts of Cosmic Dust on Planetary Atmospheres and Surfaces. *Space Sci. Rev.*, *214*(1), 23. doi: 10.1007/s11214-017-0458-1

Porco, C. C., West, R. A., McEwen, A., Del Genio, A. D., Ingersoll, A. P., Thomas, P., ... Vasavada, A. R. (2003, March). Cassini imaging of jupiter's atmosphere, satellites, and rings. *Sci*, *299*, 1541-1547.

Postberg, F., Kempf, S., Srama, R., Green, S. F., Hillier, J. K., McBride, N., & Grün, E. (2006, July). Composition of jovian dust stream particles. *Icarus*, *183*(1), 122-134. doi: 10.1016/j.icarus.2006.02.001

Redwing, E., de Pater, I., Luszcz-Cook, S., de Kleer, K., Moullet, A., & Rojo, P. M. (2022, October). NaCl and KCl in Io's Atmosphere. *Planetary Sci. J.*, *3*(10), 238. doi: 10.3847/PSJ/ac9784

Robitaille, T., Deil, C., & Ginsburg, A. (2020, November). *reproject: Python-based astronomical image reprojection.* Astrophysics Source Code Library, record ascl:2011.023.

Roesler, F. L., Moos, H. W., Oliversen, R. J., Woodward, J., R. C., Retherford, K. D., Scherb, F., ... Strobel, D. F. (1999, January). Far-Ultraviolet Imaging Spectroscopy of Io's Atmosphere with HST/STIS. *Sci*, *283*, 353. doi: 10.1126/science.283.5400.353

Roth, L., Boissier, J., Moullet, A., Sánchez-Monge, Á., de Kleer, K., Yoneda, M., ... Thorwirth, S. (2020, November). An attempt to detect transient changes in Io's SO_2 and NaCl atmosphere. *Icarus*, *350*, 113925. doi: 10.1016/j.icarus.2020.113925

Roth, L., Saur, J., Retherford, K. D., Feldman, P. D., & Strobel, D. F. (2014, January). A phenomenological model of Io's UV aurora based on HST/STIS observations. *Icarus*, *228*, 386-406. doi: 10.1016/j.icarus.2013.10.009

Schmidt, C., Schneider, N., Leblanc, F., Gray, C., Morgenthaler, J., Turner, J., & Grava, C. (2018, July). A Survey of Visible S^+ Emission in Io's Plasma Torus During the Hisaki Epoch. *JGR: Space Physics*, *123*, 5610-5624. doi: 10.1029/2018JA025296

Schmidt, C., Sharov, M., de Kleer, K., Schneider, N., de Pater, I., Phipps, P. H., ... Brown, M. (2023, February). Io's Optical Aurorae in Jupiter's Shadow. *Planetary Sci. J.*, *4*(2), 36. doi: 10.3847/PSJ/ac85b0

Schneider, N. M., & Bagenal, F. (2007). Io's neutral clouds, plasma torus, and magnetospheric interaction. In *Io After Galileo: A New View of Jupiter's Volcanic Moon* (p. 265-286). Berlin, Heidelberg: Springer Praxis Books / Geophysical Sciences. doi: 10.1007/978-3-540-48841-5_11

Schneider, N. M., Hunten, D. M., Wells, W. K., Schultz, A. B., & Fink, U. (1991, February). The structure of Io's corona. *Astrophys. J.*, *368*, 298-315. doi: 10.1086/169694

Schneider, N. M., & Trauger, J. T. (1995, Sep). The Structure of the Io Torus. *Astrophys. J.*, *450*, 450. doi: 10.1086/176155

Smith, B. A., Soderblom, L. A., Beebe, R., Boyce, J., Briggs, G., Carr, M., ... Veverka, J. (1979, November). The Galilean Satellites and Jupiter: Voyager 2 Imaging Science Results. *Science*, *206*(4421), 927-950. doi: 10.1126/science.206.4421.927

Smith, H. T., Koga, R., Tsuchiya, F., & Dols, V. J. (2022, August). Insight Into Io Enabled by Characterization of Its Neutral Oxygen Torus. *Journal of Geophysical Research (Space Physics)*, *127*(8), e30581. doi: 10.1029/2022JA030581

Smyth, W. H., & Combi, M. R. (1988a, May). A general model for io's neutral gas clouds. ii - application to the sodium cloud. *Astrophys. J.*, *328*, 888–918. doi: 10.1086/166346

Smyth, W. H., & Combi, M. R. (1988b, April). A general model for Io's neutral gas clouds. I - Mathematical description. *Astrophys. J., Suppl. Ser.*, *66*, 397-411. doi: 10.1086/191264

Smyth, W. H., & Marconi, M. L. (2003, November). Nature of the iogenic plasma source in Jupiter's magnetosphere I. Circumplanetary distribution. *Icarus*, *166*, 85-106. doi: 10.1016/S0019-1035(03)00176-3

Smyth, W. H., Peterson, C. A., & Marconi, M. L. (2011, July). A consistent understanding of the ribbon structure for the Io plasma torus at the Voyager 1, 1991 ground-based, and Galileo J0 epochs. *JGR: Space Physics*, *116*(A15), 7205. doi: 10.1029/2010JA016094

Steffl, A. J., Stewart, A. I. F., & Bagenal, F. (2004, November). Cassini UVIS observations of the Io plasma torus. I. Initial results. *Icarus*, *172*, 78-90. doi: 10.1016/j.icarus.2003.12.027

Tao, C., Kimura, T., Badman, S. V., André, N., Tsuchiya, F., Murakami, G., ... Fujimoto, M. (2016, May). Variation of Jupiter's aurora observed by Hisaki/EXCEED: 2. Estimations of auroral parameters and magnetospheric dynamics. *JGR: Space Physics*, *121*, 4055-4071. doi: 10.1002/2015JA021272

Tao, C., Kimura, T., Badman, S. V., Murakami, G., Yoshioka, K., Tsuchiya, F., ... Fujimoto, M. (2016, May). Variation of Jupiter's aurora observed by Hisaki/EXCEED: 1. Observed characteristics of the auroral electron energies compared with observations performed using HST/STIS. *JGR: Space Physics*, *121*, 4041-4054. doi: 10.1002/2015JA021271

Tao, C., Kimura, T., Kronberg, E. A., Tsuchiya, F., Murakami, G., Yamazaki, A., ... Okamoto, S. (2021, February). Variation of Jupiter's Aurora Observed by Hisaki/EXCEED: 4. Quasi Periodic Variation. *Journal of Geophysical Research (Space Physics)*, *126*(2), e28575. doi: 10.1029/2020JA02857510.1002/essoar.10504013.1

Tao, C., Kimura, T., Tsuchiya, F., Muirakami, G., Yoshioka, K., Yamazaki, A., ... Fujimoto, M. (2018, January). Variation of Jupiter's Aurora Observed by Hisaki/EXCEED: 3. Volcanic Control of Jupiter's Aurora. *Geophys. Res. Lett.*, *45*, 71-79. doi: 10.1002/2017GL075814

Thomas, N., Bagenal, F., Hill, T., & Wilson, J. (2004). The Io neutral clouds and plasma torus. In F. Bagenal, T. E. Dowling, & W. B. McKinnon (Eds.), *Jupiter. the planet, satellites and magnetosphere* (p. 561-591). Cambridge University Press.

Thomas, N., Lichtenberg, G., & Scotto, M. (2001, November). High-resolution spectroscopy of the Io plasma torus during the Galileo mission. *JGR: Space Physics*, *106*, 26277-26292. doi: 10.1029/2000JA002504

Tsang, C. C. C., Spencer, J. R., Lellouch, E., López-Valverde, M. A., Richter, M. J., & Greathouse, T. K. (2012, Jan). Io's atmosphere: Constraints on sublimation support from density variations on seasonal timescales using NASA IRTF/TEXES observations from 2001 to 2010. *Icarus*, *217*(1), 277-296. doi: 10.1016/j.icarus.2011.11.005

Tsuchiya, F., Yoshioka, K., Kimura, T., Koga, R., Murakami, G., Yamazaki, A., ... Sakanoi, T. (2018, August). Enhancement of the Jovian Magnetospheric Plasma Circulation Caused by the Change in Plasma Supply From the Satellite Io. *Journal of Geophysical Research (Space Physics)*, *123*(8), 6514-6532. doi: 10.1029/2018JA025316

Tukey, J. W. (1977). *Exploratory data analysis*. Addison-Wesley.

Van Rossum, G., & Drake, F. L. (2009). *Python 3 reference manual*. Scotts Valley, CA: CreateSpace.

Virtanen, P., Gommers, R., Oliphant, T. E., Haberland, M., Reddy, T., Cournapeau, D., ... SciPy 1.0 Contributors (2020). SciPy 1.0: Fundamental Algorithms for Scientific Computing in Python. *Nature Methods*, *17*, 261–272. doi: 10.1038/s41592-019-0686-2

Walker, A. C., Gratiy, S. L., Goldstein, D. B., Moore, C. H., Varghese, P. L., Trafton, L. M., ... Stewart, B. (2010, May). A comprehensive numerical simulation of Io's sublimation-driven atmosphere. *Icarus*, *207*(1), 409-432. doi: 10.1016/j.icarus.2010.01.012

Wilson, J. K., Mendillo, M., Baumgardner, J., Schneider, N. M., Trauger, J. T., & Flynn, B. (2002, June). The Dual Sources of Io's Sodium Clouds. *Icarus*, *157*,

476-489. doi: 10.1006/icar.2002.6821

Wilson, J. K., & Schneider, N. M. (1994, September). Io's fast sodium: Implications for molecular and atomic atmospheric escape. *Icarus*, *111*, 31-44. doi: 10.1006/icar.1994.1131

Wilson, J. K., & Schneider, N. M. (1999, July). Io's sodium directional feature: Evidence for ionospheric escape. *JGR: Planets*, *104*, 16567-16584. doi: 10.1029/1999JE900017

Witteborn, F. E., Bregman, J. D., & Pollack, J. B. (1979, February). Io - an intense brightening near 5 micrometers. *Sci*, *203*, 643-646. doi: 10.1126/science.203.4381.643

Woodward, R. C., Jr., Oliversen, R. J., Scherb, F., & Roesler, F. L. (2000, October). Synoptic Imaging of the Io Plasma Torus in [S II]: Long-term Variability. *Bull. Am. Astron. Soc.*, *32*(3). (AAS/Division of Planetary Sciences Meeting 32, poster #35.12)

Woodward, R. C., Jr., Scherb, F., & Roesler, F. L. (1994, September). Periodic intensity variations in sulfur emissions from the io plasma torus. *Icarus*, *111*, 45–64. doi: 10.1006/icar.1994.1132

Yoneda, M., Kagitani, M., & Okano, S. (2009, December). Short-term variability of Jupiter's extended sodium nebula. *Icarus*, *204*, 589-596. doi: 10.1016/j.icarus.2009.07.023

Yoneda, M., Kagitani, M., Tsuchiya, F., Sakanoi, T., & Okano, S. (2015, November). Brightening event seen in observations of Jupiter's extended sodium nebula. *Icarus*, *261*, 31-33. doi: 10.1016/j.icarus.2015.07.037

Yoshikawa, I., Suzuki, F., Hikida, R., Yoshioka, K., Murakami, G., Tsuchiya, F., ... Fujimoto, M. (2017, August). Volcanic activity on Io and its influence on the dynamics of the Jovian magnetosphere observed by EXCEED/Hisaki in 2015. *Earth, Planets and Space*, *69*(1), 110. doi: 10.1186/s40623-017-0700-9

Yoshioka, K., Murakami, G., Yamazaki, A., Tsuchiya, F., Kimura, T., Kagitani, M., ... Fujimoto, M. (2014, September). Evidence for global electron transportation into the jovian inner magnetosphere. *Sci*, *345*, 1581-1584. doi: 10.1126/science.1256259

Yoshioka, K., Tsuchiya, F., Kagitani, M., Kimura, T., Murakami, G., Fukuyama, D., ... Fujimoto, M. (2018, Oct). The Influence of Io's 2015 Volcanic Activity on Jupiter's Magnetospheric Dynamics. *Geophys. Res. Lett.*, *45*(19), 10,193-10,199. doi: 10.1029/2018GL079264

Zhang, J., Goldstein, D. B., Varghese, P. L., Gimelshein, N. E., Gimelshein, S. F., & Levin, D. A. (2003, May). Simulation of gas dynamics and radiation in volcanic plumes on Io. *Icarus*, *163*(1), 182-197. doi: 10.1016/S0019-1035(03)00050-2

Zhang, J., Goldstein, D. B., Varghese, P. L., Trafton, L., Moore, C., & Miki, K. (2004, December). Numerical modeling of ionian volcanic plumes with entrained particulates. *Icarus*, *172*(2), 479-502. doi: 10.1016/j.icarus.2004.06.016

Zook, H. A., Grun, E., Baguhl, M., Hamilton, D. P., Linkert, G., Liou, J. C., ... Phillips, J. L. (1996, November). Solar Wind Magnetic Field Bending of Jovian Dust Trajectories. *Sci*, *274*(5292), 1501-1503. doi: 10.1126/science.274.5292.1501

Zulko, Burrows, T., Earney, B., Mondéjar, Á., kerstin, Gaitán, M., ... Ørland, K. (2021, May). *johncooper199/moviepy* [Computer Software]. Zenodo. doi: 10.5281/zenodo.4781125